ISTANBUL TECHNICAL UNIVERSITY ★ GRADUATE SCHOOL OF SCIENCE ENGINEERING AND TECHNOLOGY

FILM FORMATION, MORPHOLOGICAL, OPTICAL AND ELECTRICAL PERCOLATION BEHAVIORS OF PS/MWCNT AND PS/GO NANOCOMPOSITE FILMS

M.Sc. THESIS

Barış DEMİRBAY

Department of Physics Engineering

Physics Programme

Thesis Advisor: Assoc. Prof. Dr. Şaziye UĞUR

JULY 2017

ISTANBUL TECHNICAL UNIVERSITY ★ GRADUATE SCHOOL OF SCIENCE ENGINEERING AND TECHNOLOGY

FILM FORMATION, MORPHOLOGICAL, OPTICAL AND ELECTRICAL PERCOLATION BEHAVIORS OF PS/MWCNT AND PS/GO NANOCOMPOSITE FILMS

M.Sc. THESIS

Barış DEMİRBAY
509151105

Department of Physics Engineering

Physics Programme

Thesis Advisor: Assoc. Prof. Dr. Şaziye UĞUR

JULY 2017

ISTANBUL TEKNİK ÜNİVERSİTESİ ★ FEN BİLİMLERİ ENSTİTÜSÜ

PS/MWCNT VE PS/GO NANOKOMPOZİT FİLMLERİNİN FİLM OLUŞUM, MORFOLOJİK, OPTİKSEL VE ELEKTRİKSEL PERKOLASYON DAVRANIŞLARI

YÜKSEK LİSANS TEZİ

Barış DEMİRBAY
509151105

Fizik Mühendisliği Anabilim Dalı

Fizik Programı

Tez Danışmanı: Doç. Dr. Şaziye UĞUR

TEMMUZ 2017

Barış Demirbay, a M.Sc. student of İTU Graduate School of Science Engineering and Technology student ID 509151105, successfully defended the thesis/dissertation entitled "Film formation, morphological, optical and electrical percolation behaviors of PS/MWCNT and PS/GO nanocomposite films", which he prepared after fulfilling the requirements specified in the associated legislations, before the jury whose signatures are below.

Thesis Advisor :	**Assoc. Prof. Dr. Şaziye UĞUR** ISTANBUL Technical University	.....
Jury Members :	**Assoc. Prof. Dr. Şaziye Uğur** İstanbul Technical University	.....
	Assoc. Prof. Dr. Demet Kaya Aktaş İstanbul Technical University	.....
	Prof. Dr. Selim Kara Trakya University	.....

Date of Submission : 5 May 2017
Date of Defense : 14 July 2017

To my father,

FOREWORD

First of all, I would like to express my utmost gratitude to my M.Sc. thesis supervisor, to my mentor, dear Assoc. Prof. Dr. Şaziye UĞUR for her excellent guidance, teaching enthusiasm, endless patience, rapid assistance and warmest personality. She taught me how to integrate cross disciplines, how to implement theoretical considerations into an experimental work without forgetting being a physicist, however, more important than that, how to be a good experimentalist when you study in the lab. Therefore, dear Mrs. UĞUR has always been and will always be more than an academic mentor that I respect all the time.

I would also like to express my sincere thanks to the jury members, dear Assoc. Prof. Dr. Demet KAYA AKTAŞ and dear Prof. Dr. Selim KARA for their immense support and their suggestions.

I would also like to thank Prof. Dr. Selim KARA for the electrical conductivity measurements of nanocomposite films that we produced in our lab. and Dr. Abdelhamid Elaissari for the synthesis of polystyrene latexes.

I would also like to thank to my friends and colleagues, particularly to Dr. Ahmet Ata AYHAN for his moral support and his all present motivation and to Can AKAOĞLU and Nazlı Ceren DAĞYAR for their moral support, sincere and genuine friendships.

At last, but not at least, I would like to express my endless gratitude to my family, to my dear father Halil DEMİRBAY, whose effort is no less than my mother, to my dear mother Mukadder DEMİRBAY who always stood behind me at each stage of my life and and to my dear sister, Tuğba DEMİRBAY who always encouraged me and made my time full of amazement.

July 2017

Barış Demirbay
Physics Engineer

TABLE OF CONTENTS

Page xi

ABBREVIATIONS

PS	**:** Polystyrene
CNT	**:** Carbon nanotube
MWCNT	**:** Multiwalled carbon nanotube
SWCNT	**:** Singlewalled carbon nanotube
GO	**:** Graphene oxide
PMMA	**:** Poly(methyl methacrylate)
PVP	**:** Polyvinyl pyrrolidone
VGCNF	**:** Vapor grown carbon nanofiber
UVV	**:** Ultraviolet visible
PNC	**:** Polymer matrix nanocomposite
CMN	**:** Ceramic matrix nanocomposite
MFFT	**:** Minimum film formation temperature
SEM	**:** Scanning electron micrograph
DL	**:** Deuterium lamp
HL	**:** Halogen lamp
ES	**:** Entry slot
PT	**:** Prager-Tirrel
wt	**:** Weight
vol	**:** Volume
3-D	**:** Three dimension
2-D	**:** Two dimension

SYMBOLS

I_{tr}	: Transmitted light intensity
$(I_{tr})_m$	: Maximum transmitted light intensity
I_{sc}	: Scattered light intensity
I_0	: Intensity of light beam
M_{MWCNT}	: Mass of multiwalled carbon nanotube
M_{PS}	: Mass of multiwalled carbon nanotube
T	: Temperature
T_g	: Glass transition temperature
°C	: Celcius degree
K	: Kelvin
p_c	: Percolation threshold
$p_\infty(p)$	: Percolation probability
P	: Lattice occupation probability
R	: Mass fraction
R_c	: Critical mass fraction
σ	: Electrical conductivity
σ_0	: Self conductivity
β	: Critical exponent
β_o	: Critical exponent for optical percolation
m	: Meter
nm	: Nanometer
ml	: Mililiter
S	: Siemens
kcal	: Kilocalorie
R^2	: Coefficient of determination
V	: Volume
s	: Second
g	: Gram
ΔE	: Activation energy of polymer backbone
ΔH	: Activation energy of viscous flow
ΔG	: Gibbs free energy
ΔS	: Entropy of activation of viscous flow
$R_s(\Omega)$	: Resistivity
Ω	: Ohm
k	: Boltzmann constant
T_0	: Minimum film formation temperature
T_h	: Healing temperature
L	: Length
$< l >$	: Mean free path
r	: radius
r_0	: initial radii of void

$\boldsymbol{R_0}$: Initial radii of particle
$\boldsymbol{N_0}$: Avagadro number
$\boldsymbol{\sigma(t)}$: Crossing density
$\boldsymbol{t}$: Time
$\boldsymbol{\tau}$: Reduced time
$\boldsymbol{\eta}$: Viscosity
$\boldsymbol{\rho}$: Relative density
$\boldsymbol{\gamma}$: Surface energy
$\boldsymbol{M_w}$: Average molecular weight of polymer
$\boldsymbol{M_i}$: Molecular weight of polymer chain
$\boldsymbol{w_i}$: Weight fraction of polymer chain
$\boldsymbol{M_a}$: Mass of monomer
$\boldsymbol{n}$: Degree of polymerization
$\boldsymbol{N_i}$: Number of polymer chains

LIST OF TABLES

Page

LIST OF FIGURES

Page

FILM FORMATION, MORPHOLOGICAL, OPTICAL AND ELECTRICAL PERCOLATION BEHAVIORS OF PS/MWCNT AND PS/GO NANOCOMPOSITE FILMS

SUMMARY

In this thesis work, multiwalled carbon nanotubes (MWCNTs) and graphene oxide (GO) with various mass fractions were used as nanofillers within polystyrene (PS) latex matrices to investigate their effects on film formation, morphological, optical and electrical percolation behaviors of PS/MWCNT and PS/GO nanocomposites. For this purpose, first of all, polystyrene (PS) latexes with different particle sizes were used to investigate the effect of particle size on the film formation, morphological and electrical properties of nanocomposite films impregnated with multi-walled carbon nanotubes (MWCNTs) by using the photon transmission (UVV) technique and electrical conductivity measurements. Three kinds of PS particles which have diameters of 382 nm, 480 nm and 560 nm respectively, were synthesized via emulsion polymerization technique. Three different sets of nanocomposite mixtures, each containing different amounts of MWCNT in the range between 0 and 20 wt.%, were prepared by latex technology which combines PS latex dispersion within aqueous MWCNT solutions. PS/MWCNT nano-composite films were prepared from these mixtures on glass substrates via drop-casting method and they all dried at 40 °C in the heating oven. Each dried sample was then annealed at varying temperatures between 100 °C and 250 °C for 10 min. In order to monitor film formation behavior of these nanocomposites, transmitted light intensity, $\boldsymbol{I_{tr}}$, was measured after each annealing step. It was found that film formation process for the nanocomposite films containing 382 nm of PS particles observed in the presence of (0-7.5 wt.%) MWCNT content while PS/MWCNT nanocomposite films including 480 nm and 560 nm of PS latex particles accomplished the film formation in the presence of (0-5 wt.%) MWCNT content. Film formation was not observed above these ranges for all nanocomposite films. Energies of voids closure and inter-diffusion were not change much with the increase of MWCNT indicating that film formation process is not affected by MWCNT content in the nanocomposite films. The surface conductivity, $(\boldsymbol{\sigma})$, of each annealed film at 250 °C was measured and was found to increase dramatically above a certain mass fraction of MWCNT content which corresponds to the percolation threshold of conductivity, $\boldsymbol{R_c}$. The conductivity of nanocomposite films in all sizes presented a typical percolation behavior and had a similar electrical percolation threshold of $\boldsymbol{R_c}$=1.5 wt.% as the MWCNT concentration. However, the electrical conductivity of nanocomposite films was found to increase one order of magnitude with the increase in PS latex particle size. Furthermore, the critical exponents of $\boldsymbol{\beta}$ for the electrical conductivity of the nanocomposites decreased from 2.64 to 1.19 with the increase in the particle size, indicating that percolation behavior alters depending on PS particle size. The exponents of $\boldsymbol{\beta}$ from the percolation power law both for 480 nm and 560 nm of PS/MWCNT nanocomposite systems were found to be 2.40 and 1.19, respectively, showing the formation of a 3-D network of randomly arranged MWCNTs. The nanocomposites prepared with larger PS particles showed that the

optimum results provide a good dispersion of MWCNTs in matrix and high electrical conductivity. SEM images also showed that improved MWCNT dispersion with the increase in particle size of polymer latex was found to be consistent with the experimental results.

As a second stage of this thesis work, the effect of graphene oxide (GO) nanoparticles on film formation behavior of PS/GO nanocomposite films composed of polystyrene (PS) latex and graphene oxide at various concentrations was investigated by using photon transmission (UVV) and scanning electron microscopy (SEM) techniques. Water-borne PS/GO nanocomposite films were prepared by emulsion mixing of PS latex and GO nanofillers at various weight percents. GO was firstly diluted and mixed with PS latex dispersions at eight different GO contents in the range between 0 and 100 wt%. SEM micrographs and conductivity measurements were also taken to evaluate the effects of GO content on the morphology and electrical properties nanocomposite films. The results showed that the addition of GO to neat PS latex has no influence on the film formation behavior of PS latex. The results of optical experiments and SEM images indicated that film formation stages of PS/GO nanocomposites are independent of weight fraction of GO, whereas its conductivity values decreased about one order of magnitude with the increase in GO content. It was found that the resultant PS/GO nanofilms possess very low amounts of conductivity values such as 10^{-13}-10^{-14} S and their optical transmission values was found over than 90% at a typical wavelength of 500 nm.

PS/MWCNT VE PS/GO NANOKOMPOZİT FİLMLERİNİN FİLM OLUŞUM, MORFOLOJİK, OPTİKSEL VE ELEKTRİKSEL PERKOLASYON DAVRANIŞLARI

ÖZET

Son yıllarda özellikle endüstride boya, mürekkep, su bazlı yapıştırıcı ve tekstil malzemesi olarak kullanılan polimer lateksler farklı mühendislik alanlarında da büyük avantajlar sağlamaktadır. Lateksler su, oksijen ve korozyona neden olabilecek pek çok organik çözücü ortamında dayanıklılığı yüksek olan ancak filmleşme sonrası mekanik dayanımı konvansiyonel polimerlere göre daha düşük olan malzemelerdir. Film oluşturma süreçleri pratik ve kolay olduğu için aynı zamanda kaplama malzemesi olarak kullanılmaktadırlar. Camsı geçiş sıcaklıklarının derecesine bağlı olarak yumuşak veya sert lateksler olarak sınıflandırılırlar. Camsı geçiş sıcaklığı, oda sıcaklığının altında olan lateksler kolaylıkla filmleşebiliyorsa, bu tür latekslere yumuşak lateksler denir. Eğer lateksler bu değerin çok üstünde bir sıcaklık değerinde filmleşme özelliği gösteriyorsa, bu tür lateksler sert lateksler olarak adlandırılırlar.

Film oluşum süreçleri ve filmleşmenin takibi kaplamanın kalitesini belirleme ve karakterizasyonu açısından oldukça önemlidir. Polimer latekslerde filmleşme süreçleri kısaca 4 temel aşamayla özetlenebilir. Lateks ile kaplanan yüzey sıcaklık verildiğinde içindeki su buharlaşarak kolloid yapılı moleküller bir araya toplanır. Artan sıcaklıkla birlikte parçacık deformasyonu başlayarak birbirine yanaşan moleküller arası boşluklar kapanarak bal peteği formunu alır. Daha yüksek sıcaklık değerlerinde ise moleküller arası kaynaşma ve inter-difüzyon mekanizmaları başlayarak homojen film yapılarının ortaya çıkması sağlanarak filmleşme süreci tamamlanır. Filmleşme sonucu ortaya çıkan filmin transparanlığı (optiksel geçirgenlik değeri) mühendislikte uygulanabilirliği açısından büyük önem taşır. Ancak, elde edilen filmlerin tek başına yüksek optiksel geçirgenlik değerlerine sahip olmaları her zaman katkı sağlamaz.

Polimerlerin daha fonksiyonel bir biçimde kullanılabilmesi açısından polimer çözeltilerinin içine karıştırılan katkı fazları, ortaya çıkan ürünün pek çok üstün özellik kazanmasını sağlar. Polimer matrislerin içerisine uygun kompozisyonda katılan katkı malzemeleri boyutlarına bağlı olarak kompozit veya nanokompozit yapıların ortaya çıkmasına neden olur. Bu sayede polimerler tek başına sahip olamadıkları özelliklere sahip daha güçlü yapılara dönüşmektedir. Özellikle son yıllarda, karbon bazlı katkı malzemeleri kompozitlerin mekaniksel dayanımını, termal ve elektriksel iletkenlik özelliklerini artırmak amacıyla sıklıkla kullanılmaktadırlar. Bu katkı malzemelerinin polimer matrisler içerisindeki homojen dağılımları pek çok basit kimyasal, fiziksel yöntemle veya uyumlaştırıcıların yardımıyla mümkündür. Bu sayede katkılama fazının dispersiyon kalitesine bağlı olarak ortaya çıkan kompozit malzemelerin özellikleri yükseltilebilir.

Yüksek sıcaklık değerlerinde optiksel geçirgenlik değerleri yüksek olan polimerler göz önüne alındığında, hem transparanlık hem de elektriksel iletkenlik değerleri yüksek yapılar elde edilebilmektedir. Polistiren (PS) gibi sert latekslerden elde edilen filmler yüksek sıcaklıklarda transparanlaşarak optiksel geçirgenlik değerleri %90'a kadar

ulaşabilmektedir. Özellikle son yıllarda, elektriksel iletkenlik özellikleri açısından yaygınca kullanılan çok duvarlı karbon nanotüp (MWCNT) ve grafen oksit (GO) gibi malzemeler, yüksek sıcaklık değerlerinde transparan hale dönüşen polimer latekslerin ortamında fonksiyonel kompozit yapıların ortaya çıkmasını sağlamaktadır. Bu nedenle polistiren lateks matrislerinden oluşan karbon nanotüp ve grafen oksit katkılı kompozitlerin kullanılması optoelektronik uygulamalarında büyük potansiyele sahiptir.

Bu tez çalışmasında, çeşitli konsantrasyon değerlerinde (kütle fraksiyonlarında) hazırlanmış olan çok duvarlı karbon nanotüp ve grafen oksit çözeltileri polistiren lateks matrisi içinde katkılama fazı olarak kullanılmış olup, bu malzemelerden elde edilmiş olan PS/MWCNT ve PS/GO nanokompozit filmleri üzerinde film oluşum süreçleri, morfolojik özellikler, optiksel ve elektriksel perkolasyon davranışlar araştırılmıştır. Bu amaca yönelik olarak öncelikle farklı büyüklük değerlerine sahip olan polistiren latekslerin parçacık boyutunun, çok duvarlı karbon nanotüp katkılı nanokompozit filmler üzerindeki davranışları foton geçirgenlik testi, taramalı elektron mikroskobu (SEM) ve elektriksel iletkenlik ölçümleri referans alınarak çalışılmıştır.

Tez çalışmasının ilk aşaması olarak, 382 nm, 480 nm ve son olarak 560 nm büyüklük değerlerine sahip polistiren latex parçacıklar farklı oranlarda uyumlaştırıcı kullanılarak emülsiyon polimerizasyon tekniği ile sentezlenmiştir. %0 ve %20 değer aralığında pek çok farklı kütle fraksiyonunda hazırlanan sulu çok duvarlı karbon nanotüp çözeltileri, farklı boyutlarda sentezlenmiş olan polistiren latekslerle karıştırılarak hazırlanmıştır. Polistiren lateks ve çok duvarlı karbon nanotüp çözeltilerinden oluşan PS/MWCNT nanokompozit filmleri damlatma yöntemi kullanılarak ısıtma fırını içerisinde 45 °C'de cam substratların üzerine eşit şekilde damlatılarak kaplanmıştır. Bu sıcaklık değerinde kurutulan her bir film örneği 100 °C'den 250 °C'ye farklı sıcaklık aralıklarında 10'ar dakika tavlanmıştır. Film oluşum süreçlerini gözlemlemek amacıyla, hazırlanan tüm numunelere foton geçirgenlik testi uygulanarak optiksel geçirgenlik değerleri her farklı sıcaklık değerinde ölçülmüştür. Ölçüm sırasında, bu malzemelerden oluşan nanokompozit filmler için UV spektrometrenin dalga boyu değeri 500 nm olarak belirlenmiştir. Çünkü 500 nm'de polistiren ve çok duvarlı karbon nanotüpler için spesifik bir absorpsiyon değeri yoktur.

Deney sonuçlarına göre, 382 nm polistiren lateks parçacıklarından oluşan nanokompozit filmler film oluşum sürecini %0 ve %7.5 aralığındaki çok duvarlı karbon nanotüp varlığında tamamlarken, 480 nm ve 560 nm lateks parçacıklarından oluşan numuneler bu süreci yalnızca %0 ve %5 aralığındaki çok duvarlı karbon nanotüp ortamında tamamlamaktadır. Film oluşum süreçleri, belirtilen bu konsantrasyon değerlerinin üzerinde gerçekleşmeye devam etmesine karşın, kullanılan katkı fazının yoğunluğu nedeniyle transparanlığı neredeyse %0'a düşürmüştür. Boşlukların kapanması, kaynaşma ve kolloidal lateks parçacıklarının içinde yer alan polimer zincirlerinin inter-difüzyonu sonucu hesaplanmış olan viskoz akış aktivasyon enerjisi ve birbiriyle kaynaşan polimerlerin belkemiği (backbone) hareket aktivasyon enerjisi kullanılan çok duvarlı karbon nanotüplerin kütle fraksiyonuna bağlı olarak çok büyük bir artış göstermemektedir. Bu durum, kullanılan güçlendirme faz miktarının filmleşme sürecini çok fazla etkilemediğini göstermektedir. Bunun yanı sıra, 250 °C'de tavlanmış olan her bir nanokompozit numunenin yüzey iletkenlik değerleri ölçülmüş olup, kritik konsantrasyon değeri (perkolasyon eşik değeri) üzerinde elektriksel iletkenlik değerlerinin hızla büyük oranda arttığı gözlemlenmiştir. Deney sonucu olarak, farklı boyutlarda polistiren latekslerden oluşan nanokompozit film

setleri aynı tip perkolasyon davranışı göstermiş olup, çok duvarlı karbon nanotüp için perkolasyon eşiği %1.5 konsantrasyon değeri olarak belirlenmiştir. Perkolasyon eşiğinin polistiren parçacık boyutundan etkilenmediği açıkça anlaşılmıştır.

Ancak, elektriksel iletkenlik değerleri polistiren latekslerin parçacık boyutunun artmasıyla birlikte artış göstermiştir. Perkolasyon hesabına bağlı olarak bulunan ve boyutu temsil eden kritik üsler, parçacık boyutunun artması ile birlikte 2.64'ten 1.19'a kadar düşmüştür. 480 nm ve 560 nm boyutlarındaki polistiren latekslerden oluşan nanokompozit filmler sırasıyla 2.40 ve 1.19 kritk üs değerlerine sahip olup bu değerler, fiziksel anlamda nanokompozit yapıda 3 boyutlu çok duvarlı karbon nanotüplerin oluşturduğu ağ yapısına karşılık gelmektedir. Daha büyük boyutlardaki polistiren latekslerin, çok duvarlı karbon nanotüplerin varlığında daha iyi dağılım gösterdiği ve daha yüksek elektriksel iletkenlik değerlerine sahip olduğu deneysel olarak gözlemlenmiştir. Kompozit yapının içine katılan çok duvarlı karbon nanotüplerin miktarına bağlı olarak, perkolasyon teorisi saçılan ışık şiddetine uyarlanarak optiksel perkolasyonlar hesaplanmıştır. Elektriksel perkolasyonda olduğu gibi, optiksel perkolasyon hesabında da optiksel perkolasyon eşiği %1.5 olarak hesaplanmıştır. Bulunan kritik üsler neredeyse birbirine çok yakın olup, kullanılan katkı fazından etkilenmediği ortaya çıkmıştır. Hazırlanan filmlerin taramalı elektron mikroskobu (SEM) görüntüleri, deneysel sonuçları doğrulayacak nitelikte olup, lateks parçacık boyutunun artmasının çok duvarlı karbon nanotüpler için daha iyi dağılım ortamı yarattığını açıkça göstermektedir. Karbon nanotüp miktarının artışına bağlı olarak, optiksel geçirgenlik değerinde deneysel olarak gözlemlenen düşüş, SEM fotoğraflarında gözlenen karbon nanotüp topaklanmalarıyla da doğrulanmıştır.

Tezin ikinci aşaması olarak, grafen oksit (GO) moleküllerinin polistiren lateks çözeltisi içerisinde kullanılarak film oluşum süreçlerine ve elektriksel özelliklerine nasıl etki ettiği araştırılmıştır. Bu çalışmada, 540 nm boyutlarında kolloidal polistiren lateks parçacıkları kullanılmış olup, farklı konsantrasyonlarda grafen oksit çözeltisi polistiren latekslerle karıştırılmıştır. Film oluşum süreçleri ve elektriksel özellikleri foton geçirgenlik testi taramalı elektron mikroskobu (SEM) görüntüleri ve iletkenlik ölçüm sonuçları ile takip edilmiştir. İlk olarak grafen oksit belli miktarda saf su kullanılarak seyreltilmiş olup, %0 ve %100 değer aralığında 8 farklı konsantrasyon değeri belirlenerek polistiren çözeltileri ile karıştırılmıştır. Ultrasonikasyon yöntemi uygulanarak grafen oksitlerin lateksler içerisinde dispersiyonu sağlanmıştır. Foton geçirgenlik testinde 550 nm dalga boyu uygulanmış olup, bu değerde grafen oksit'in spesifik bir absorbsiyonu bulunmamaktadır.

Deneysel olarak farklı konsantrasyon değerlerinde katılan grafen oksitlerin PS/GO nanokompozitlerinin filmleşme sürecini gözle görülür bir şekilde etkilemediği anlaşılmıştır. Filmleşme süreçleri, hesaplanan viskoz akış aktivasyon enerjisi ve belkemiği hareketi aktivasyon enerji değerleri, kullanılan katkılama fazından neredeyse tamamen bağımsız olup, elektriksel iletkenlik değerlerinin düşmesine neden olmuştur. Tavlanan filmlerin optiksel geçirgenlik değerleri (transparanlığı) neredeyse %90'ın üzerinde olmasına rağmen, elektriksel iletkenlik değerleri 10^{-13} ve 10^{-14} S aralığında değişmektedir.

1. INTRODUCTION

Nanotechnology, the study and the implementation of science conducted at the nanoscale, is one of the most promising branches of the science encompassing the study fields ranged from physics to almost all engineering disciplines for the progress of the latest technology [1]. Today, a broad range of the engineered structures, semiconductor devices and synthesized materials which are widely used in microelectronics, composite films, tissue engineering, drug delivery, biotechnology and so forth, have been manufactured as a result of the manipulation of matter where at least one of the dimensions is ranged between 1 and 100 nanometers [2]. Particularly, nanomaterials which possess an average grain size less than 100 nanometers [3], exhibit remarkable characteristics that directly affect physical, chemical and even biological properties of the medium that renders them in the case of their appropriate utilization at the nanoscale. Based on recent studies in the literature, as nanomaterials have a greater surface area with respect to volume ratio when it is compared to conventional forms, they show unique chemical reactivity, better mechanical, electrical and optical properties [4]. Nanomaterials can basically exist either in single, fused, aggregated or agglomerated forms with various shapes such as spherical, tubular or irregular. Both physical and chemical characteristics of nanomaterials are strongly dependent on their size, shape and morphology at the nanoscale. Therefore, unlike bulk, micro-structured conventional materials, some specific characteristics of nanomaterials such as electrical conductivity, mechanical strength or even electronic structure shows prominent difference owing to high surface energy, the spatial confinement which leads to quantum effects, reduced imperfections and a large fraction of surface atoms [5]. The classification proposal of nanostructured materials was firstly considered by Gleiter in 1995 [6] which then it was explained with the further details by Skorokhod in 2000 [7] without consideration of some special structures as nanostructured materials at different dimensions such as fullerenes, nanotubes and so on. Afterwards, nanostructured materials were classified by the contributions of two significant scientists, Pokropivny and Skorokhod [8], into

four essential categories on the basis of the number of dimensions which are zero-dimensional (quantum dots, atom clusters, heterogeneous particles arrays, core-shell quantum dots) [9], one-dimensional (nanowires, nanorods, nanotubes, nanobelts, nanoribbons) [10], two dimensional (branched structures, nanoplates, nanosheets, nanowalls, nanodisks) [11] and three dimensional (nanoballs, nanocoils, nanocones, nanopillers, nanoflowers) [12] nanostructured materials, respectively. In parallel with emerging of nanomaterials, integration of them as the reinforcing phase in the presence of other materials leads to the big reveal of the definition entitled nanocomposites. Nanocomposites are basically the composite materials consist of reinforcing phase and matrix phase where at least one of the phases is of the order of a nanometer (nm) [13]. Microcomposites have some limitations like having high anisotropy based upon the orientation of fibers and losing of optical, electrical and chemical properties in time during the applications. Nanocomposites can thus be an alternative to get rid of these limitations as distinct from microcomposites since they possess large amounts of interfacial area and short distances between reinforcing fillers [14]. Nanocomposites can be classified into three different categories based on the material used as a matrix, which are polymer matrix nanocomposites (PNCs), ceramic matrix nanocomposites (CMNs) and metal matrix nanocomposites (MMNs), respectively. Particularly in the last 20 years, PNCs and their functionality have attracted a great attention by an important part of researchers in the world as polymers are mostly flexible, easy to produce, easily processed and low cost materials [15,16]. Today almost all types of polymers involving thermosets, thermoplastics and elastomers are being used in PNCs with various reinforcing agents in such forms of particles, platelets or fibers [17]. Mechanical, thermal, electrical and optical characteristics of PNCs can be enhanced based on interfacial interactions between nano-reinforcements and polymer matrix, dispersion state of nanofillers and matrices, processing techniques and polymerization methods. Besides, the effectiveness of reinforcing phase for tailoring the characteristics of PNCs and the provision of high energy surfaces, is strongly dependent on the proportion of surface area of filler with respect to its volume [18]. It is also believed that conformations of polymers and dynamics of polymer chains are strongly affected by the confinement of polymer chains and polymer-surface interactions [19]. Thus, the dispersion state and the form of used polymers as polymer matrices in PNCs are significant as well to obtain the resultant products. For this reason, the appropriate use of polymer latexes in PNCs are of a great interest for

researchers rather than conventional polymer networks. Polymer latexes essentially consist of very fine polymer particles in the form of colloids which are well-dispersed in a carrier medium. Nowadays, polymer latexes have been utilized in many different branches of the industry as water-based adhesives, inks, paints, textiles but most importantly coating materials in films [20,21]. In essence, polymer latex films in dried forms do not have strong mechanical properties, however, they are great resistive in the presence of organic solvents, water, oxygen and other abrasive materials [22]. Latexes used as film coatings can be made up of soft or hard polymer particles. Soft latex polymer particles have a glass transition temperature (T_g) below room temperature while hard polymer particles have high-T_g [23]. Latex films generally refer to the films consisting of aqueous dispersions of soft polymer particles (low-T_g). Film formation process of soft and hard polymer latexes shows a prominent difference. For low-T_g latexes, the forces which accompany the evaporation of water are well-enough to deform the particles into void-free, optically transparent film. Differently, for latex films from hard polymer particles, the particles remain un-deformed and discrete in the drying process. In such films, the evaporation of solvent during annealing process results in firstly void closure, then healing and inter-diffusion of chains across particle-particle boundaries [24]. After film formation process, transparency of the resultant micro or thin films containing polymers or polymer latexes is a great characteristic to be considered both for industrial and scientific applications such like optoelectronics. However, polymers and polymer latexes do not solely sufficient to ensure multifunctional characteristics and to be utilized in high demand applications. In this case, the addition of inorganic or organic nano-fillers into polymer latexes for the purpose of enhancement in electrical, mechanical or even optical properties is the best way of making polymer latexes versatile materials. Especially, carbon-based nano-fillers have garnered a considerable attention by polymer science community rather than the use of conventional inorganic fillers in polymer matrices. A number of reviews and experimental outcomes in the literature indicate that carbon nanotubes (CNT) and graphene oxide (GO) are widely used as carbon-based nano-fillers in PNCs to provide the improvement considering mechanical, thermal, electrical conductivity, flame retardancy properties [25]. On the other hand, the state of dispersion and proper exfoliation of these nano-fillers within the polymer matrix to enhance the quality of PNCs are still controversial issues for

researchers based on the viscosity of the medium, polymerization techniques and types of polymer matrices. It is obvious that CNTs and GO display an efficient compatibility with organic polymers [26-28]. Therefore, application of latex technology is a great approach for such organic polymers like polystyrene (PS) to incorporate CNTs and GOs within PNCs. PS latexes can be easily produced via emulsion polymerization technique which results in very fine PS particles dispersed in a solvent where CNTs and GO fill the voids between particles. Homogeneous dispersion of CNTs and GOs which have high electrical conductivity within insulating PS latexes leads to three-dimensional (3-D) conductivity network which is described by percolation theory [29]. At a critical value of the mass fraction of CNT or GO which corresponds to percolation threshold, electrical conductivity dramatically increases with very high orders of magnitude. In general, electrical conductivities of CNTs and GOs are considerably high at very low percolation thresholds, indicating that their utilization as nano-fillers is very convenient for applications in the presence of polymer latexes. At this point, the foremost advantage of PS latexes is to obtain optically transparent nano-composite films containing low mass fractions of CNTs and GOs above their T_g. As a consequence, PS/CNT and PS/GO nano-composites including very low amounts of CNT and GO within PS latex dispersions are a great deal of interest to produce highly conductive and optically transparent films for broad range applications. However, film formation mechanisms, percolation behaviors, dispersion of conductive fillers in polymer matrices are playing a significant role to tailor the quality of resultant films on the surface of substrates. In this thesis work, film formation phenomena considering voids closure and inter-diffusion processes, optical and electrical percolation behaviors and electrical conductivity properties of PS/MWCNT and PS/GO nano-composite films were studied. In nanocomposite films, multi-walled carbon nanotubes (MWCNTs) and graphene oxide (GO) were used as nano-filler in PS latexes as their utilization can lead to enhancement in electrical conductivity and optical transparency. For PS/MWCNT nanocomposite films, polystyrene (PS) latexes with different particle sets which are 382 nm, 480 nm and 560 nm, respectively were used while 540 nm of PS latexes were used in PS/GO nanocomposites. Photon transmission (UVV) technique, scanning electron micrographs (SEM) and electrical conductivity measurements were considered for their characterization.

2. BASIC DEFINITIONS

2.1 Polymer

Polymers, also known as macromolecules, are basically a large group of molecules which are composed of repeating structural units called monomers generally linked to each other by covalent bonds. Repeating units are mostly consisting of carbon and hydrogen atoms, however, in some cases, they can also contain such kind of molecules or atoms like oxygen, nitrogen, phosphorous, silicon and so forth. Specifically, some polymers include only carbon and hydrogen atoms which refer to organic polymers. Organic polymers, such as polyethylene, polybutylene, polystyrene, are essentially made of carbon atoms which are bonded together to form long chains called the backbone of the polymer. One or more atoms can easily connect to the carbon atoms in the backbone to form side groups on polymer structure. The polymers that have a silicon or phosphorous backbone rather than having long carbon chains, can be considered as inorganic polymers. Polymers can be synthesized to obtain desired feature and functions to be used in a set of applications by considering many diverse polymerization techniques.

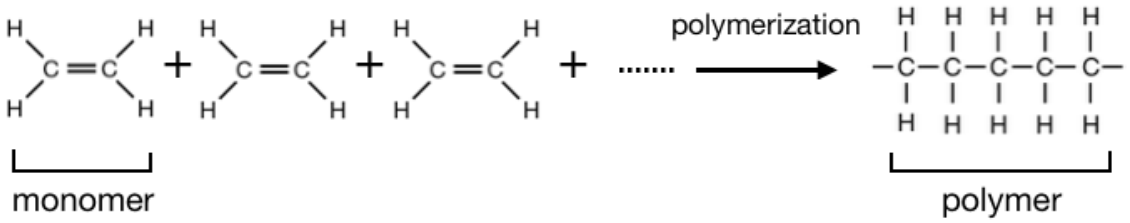

Figure 2.1 : Formation of polyethylene from ethylene monomers via polymerization process.

Condensation polymerization, chain growth polymerization and emulsion polymerization are intensively applied as chemical techniques to ensure the formation polymeric chains with different molecular weights between the monomers. After polymerization process, the average molecular weight of the resultant polymer can be calculated by the following formula:

$$M_w = \sum w_i M_i \tag{2.1}$$

where M_w is the average molecular weight, w_i is weight fraction of chains with molecular weight M_i, and M_i is molecular weight of chains. The number of monomers in the monomer chain is called the degree of polymerization and it is denoted by "n". Mass of polymer, M_n, can be calculated by the multiplication of the degree of polymerization, n, and mass of monomer, M_a, as follows:

$$M_n = nM_a \tag{2.2}$$

Determination of the exact value of polymer mass is one of the challenging issues. Thus, the statistical distribution of the length of formed polymer chains during the polymerization process is considered.

The length of polymer chain can be defined through average molecule mass in terms of numbers and distribution of average molecular mass by means of weight. If there is N_i of the chains with molecular mass, M_i, average molecule mass in terms of numbers can be calculated by the following formula:

$$M_n = \frac{\sum N_i M_i}{\sum N_i} \tag{2.3}$$

and the average molecule mass by means of weight can be calculated as follows:

$$M_w = \frac{\sum W_i M_i}{\sum W_i} \tag{2.4}$$

where $W_i = N_i M_i$. Based on polymerization or any chemical reaction, polymers can form a larger group of molecules called macromolecules. Macromolecules can consist of the same or different molecules. Polymers of the same kind of molecules are called homopolymer while polymers of different type of molecules are called copolymer. Polymers can also be classified into three categories on the basis of their conformations which are linear polymers, branched polymers and cross-linked polymers respectively.

Flexible and long chained polymers can be randomly oriented and entangled in molecular level and the movement of polymer molecule initiates above or near glass transition temperature (T_g). Disordered entanglements and random orientation result in amorphous structured polymers which are more transparent, easy to melt and soften at high temperatures. As distinct from amorphous polymers such as polystyrene, some

polymers are highly oriented side by side and their parallel chains pack very tightly to form crystalline structures depending on the degree of crystallinity.

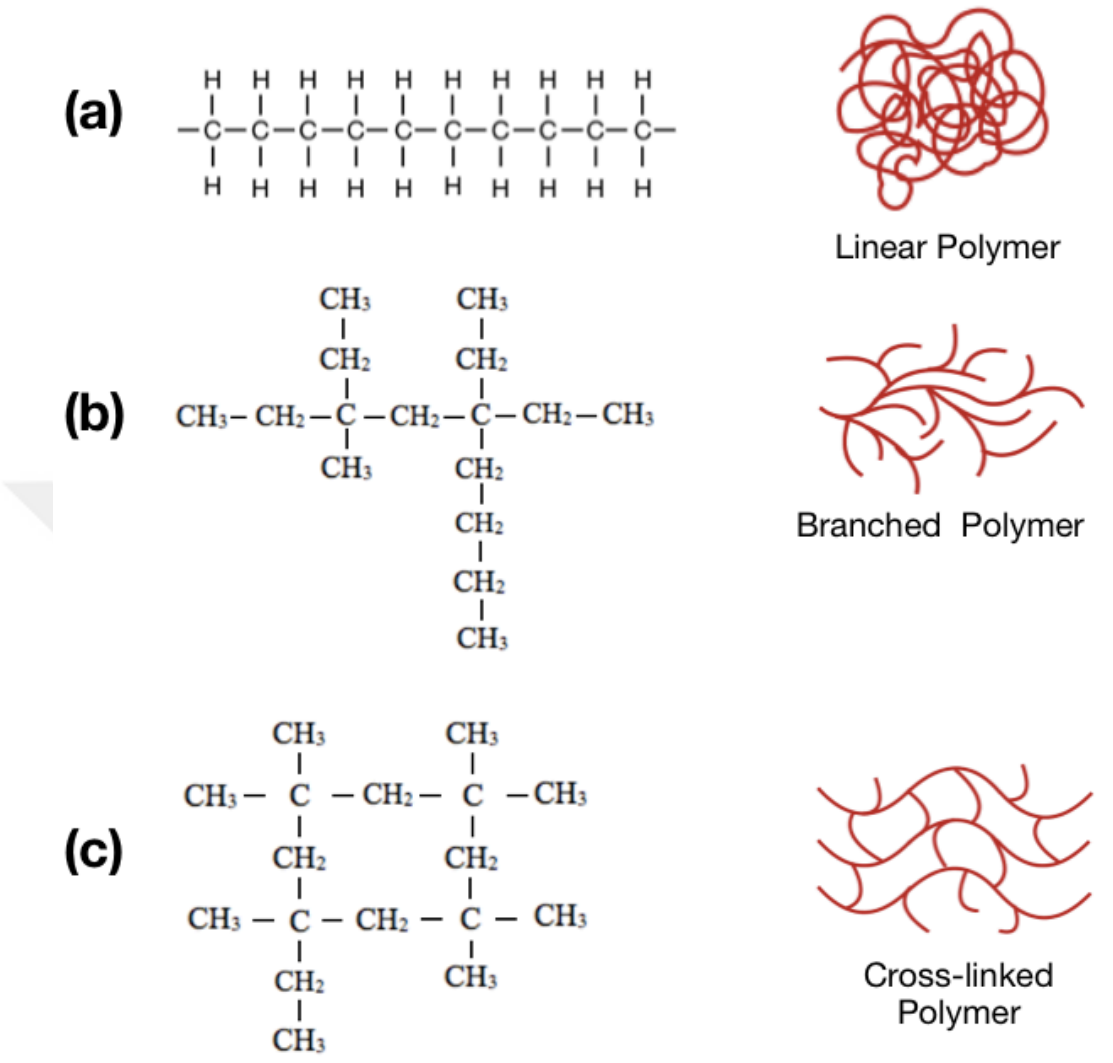

Figure 2.2 : A schematic illustration of (a) linear polymers, (b) branched polymers and (c) cross-linked polymers.

The crystalline morphology and the degree of crystallinity of a polymer can be tailored based on cooling and melting conditions. At this point, polymers can be divided into two essential categories on the basis of their reproducibility by re-heating process which are thermoplastics and thermosets. Thermoplastic polymers like polyethylene, are also be branched or linear structured polymers, can be molded and remolded into different forms when the heat is given. Besides, thermoset polymers such as resin can not melt once formed and reprocessed by reheating process since it leads to irreversible chemical reaction. In this thesis work, amorphous polystyrene particles used in the form of the polymer latex. Therefore, further information about polymer latexes was given in the following headline.

2.2. Polymer Latex

Polymer latexes which are widely used in paints, inks, coatings and drug delivery, are basically made of very fine polymer particles in the form of colloids uniformly dispersed within a solvent medium. All type of latex particles keeps their solid state below glass transition temperature (T_g). Latex particles composed of two parts: main polymer and different kind of polymer employed as a shell to encapsulate the main polymer from the outside [30,31]. Aqueous latexes have polymer particles which are well-dispersed in water while non-aqueous latexes are not uniformly dispersed in water. For the homogeneous composition of polymer particles in non-aqueous latexes, the quality of the solvent should be greater than the polymer used as a shell. In this solvent, the main polymer particles get away from each other as the occurrence of the steric barriers arising from the polymer chains on the shell.

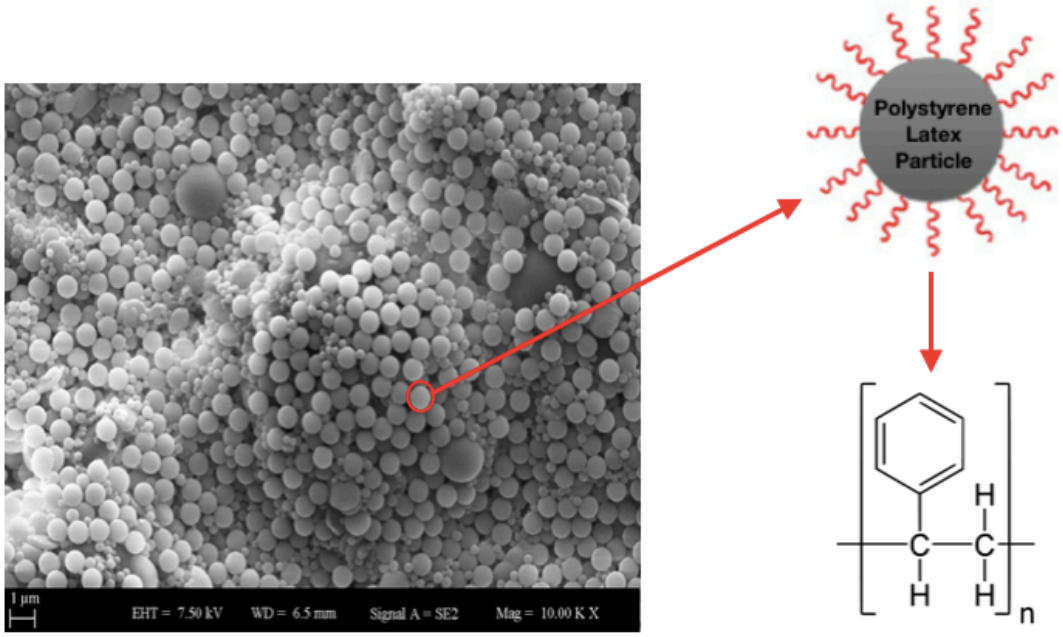

Figure 2.3 : SEM image and chemical formula of polystyrene (PS) latex particles.

The second way to obtain the uniform dispersion of polymer particles within latex is to use an appropriate surfactant depending on the solvent medium and the type of shell-polymer. When an organic solvent including latex particles is dropped onto a flat surface if transparent and continuous films are obtained after the evaporation of a solvent, such latexes are called as soft latexes. Minimum film formation temperature (MFFT) for soft latexes is generally at or below room temperature. If there is no deformation after evaporation of a solvent, such latexes are defined as hard latexes. T_g

of hard latexes is well above room temperature. In this thesis work, polystyrene (PS) particles which are synthesized via emulsion polymerization technique were used as hard polymer latex in nanocomposite films.

2.3 Polymer Nanocomposites (PNCs)

Composites are a new emerging class of materials which consist of two or more constituent compounds having different chemical and physical characteristics. The composition of multiple compounds such as polymers in the presence of reinforcing phase results in the structures with advanced functions. Particularly in last two decades, the utilization of polymer composites is considerably increased for the manufacturing of industrial and daily products such as sporting stuff, automobiles, aerospace materials and so on since polymers are light weight and corrosion-resistant materials.

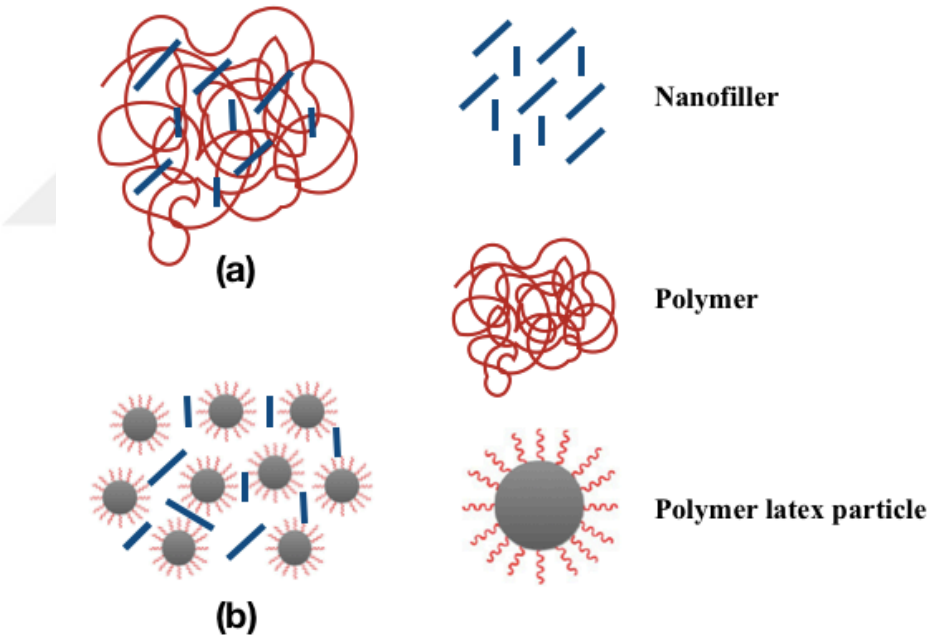

Figure 2.4 : A schematic representation of (a) conventional polymer matrix nanocomposites and (b) polymer latex matrix nanocomposites.

However, more important than that, the transition of reinforcing fillers from micro form to nano form gives rise to change in characteristics of the resultant structures. Such materials are called as nanocomposites. Polymer nanocomposites (PNCs) are essentially composed of a polymer matrix and well-dispersed or embedded nanofillers within polymer matrices where at least one dimension is must be in the range between 1 nm 50 nm. Nanofillers which are aimed to be used as reinforcing phase can be in the

form of platelets, fibers and spheroids. In polymer nanocomposites, surface area to volume ratio increases as the size of reinforcing particles gets smaller. Higher surface area of polymer leads to ease in interactions of particles within the composition as well. Therefore, such properties like strength, heat resistance and electrical conductivity of nanocomposites remarkably increase depending on particle size of the used fillers. In the Figure 2.4, the simple cartoon representation of nanocomposites is shown.

3. THEORETICAL CONSIDERATIONS

3.1 Film Formation Phenomena

3.1.1 Void closure

Latex deformation and void closure between polymer particles can be induced due to shearing stress generated by the surface tension of polymer refer to polymer-air interfacial tension. The void closure kinetics can detect the time for film formation in latex and the optical transparency [32]. To relate the shrinkage of the spherical void of radius, r to the viscosity of surrounding medium, an η expression can be derived and can be given as follows [33]:

$$\frac{dr}{dt} = -\frac{\gamma}{2\eta}\left(\frac{1}{\rho(r)}\right) \tag{3.1}$$

where γ is surface energy, t is time and $\rho(r)$ is the relative density. It should be noted that surface energy leads to a decrease in size of void and the term of $\rho(r)$ varies depending on the micro structural characteristics of the material, such as the number of voids, packing and the initial particle size.

Equation 3.1 is similar to one, which is used to examine the time dependence of the minimum film formation temperature during film formation process in latex [34]. If the viscosity is assumed to be constant in time, the integration of Equation 3.1 gives the following relation

$$t = -\frac{2\eta}{\gamma}\int_{r_0}^{r}\rho(r)dr \tag{3.2}$$

where r_0 is the initial void radius at time $t = 0$. A decrease in void size (r) leads to an increase in mean free path, $< l >$, of a photon that results in an increment in transmitted light intensity, I_{tr}. This phenomena can be described by Frenkel's neck formation model by considering identical contacting polymer spheres under the effect of surface tension. At this point, Frenkel's model declares that the displaced volume is redistributed in a uniform fashion and remaining surfaces keep their original shapes with a larger radii

which which allows the formation of larger mean free path, $< l >$, of a photon. Frenkel's neck formation process is given in figure:

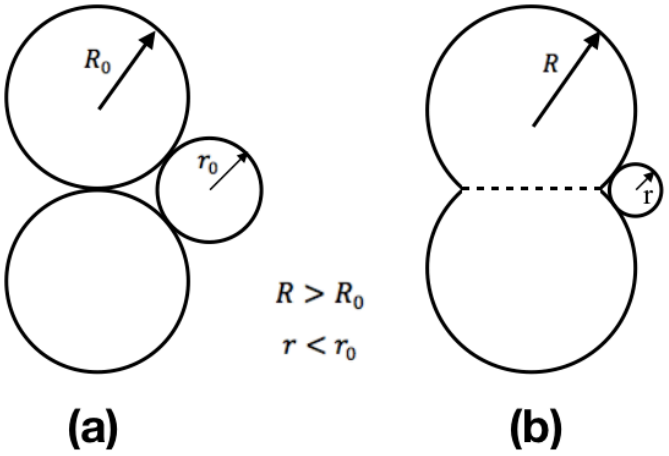

Figure 3.1 : Geometrical representation of Frenkel's neck model: (a) before and (b) after neck growth. R_0, R and r_0 are the particle and void radii before and after neck growth.

The dependence of the viscosity of polymer melt on temperature is influenced by coping with the forces of macromolecular interaction which let the segments of polymer chains jump over from one equilibration position to another one.

This process takes a place at temperatures where free volume becomes large enough and is linked with the overcoming of the potential barrier. The theory of Frenkel-Eyring reveals the relation which is given below for the temperature dependence of viscosity [35-37].

$$\eta = (N_0 h/V) exp(\Delta G/kT) \tag{3.3}$$

where N_0 is Avagadro's number, h is Planck's constant, V is molar volume and k is Boltzmann constant. It is known very well from statistical physics that $\Delta G = \Delta H - T\Delta S$, then Equation 3.3 can be written in the form of:

$$\eta = Aexp(\Delta H/kT) \tag{3.4}$$

where ΔH is the activation energy of viscous flow which refers to the amount of heat that has to be given to one mole of material to create the act of a jump during viscous flow. ΔS is the entropy of activation of viscous flow. A denotes a constant for the related parameters that independent of the temperature. If the Equations 3.2 and 3.4 are combined, the following useful equation can be expressed as follows:

$$t = -\frac{2A}{\gamma} exp\left(\frac{\Delta H}{kT}\right) \int_{r_0}^{r} \rho(r) dr \tag{3.5}$$

In order to quantify the results found above, Equation 3.5 can be employed by considering the interparticle voids are in equal size and number of voids keeps constant during the film formation process (i.e. $\rho(r) \alpha r^{-3}$), then integration of Equation 3.5 gives a new relation as follows:

$$t = \frac{2AC}{\gamma} exp\left(\frac{\Delta H}{kT}\right)\left(\frac{1}{r^2} - \frac{1}{{r_0}^2}\right) \tag{3.6}$$

where, C is a constant related to relative density $\rho(r)$.

3.1.2 Healing and inter-diffusion

The increase in I_{tr} above T_h temperature was explained in the section of void closure, through the increment in the transparency of latex film owing to the vanishing of the deformed particle-particle interfaces. Since the annealing temperature is increased above healing temperature, T_h, some part of the polymer chains may cross the junction surface and particle boundaries begin to disappear, as a result I_{tr} increases on account of the shorter optical and long mean free paths of a photon [38-42].

In order to quantify these results, the Prager-Tirrell (PT) model [43] can be employed to explain the chain crossing density. These authors used de Gennes's "reptation" model for the reveal of configurational relaxation at the polymer-polymer junction in which each polymer chain is assumed to be confined to a tube where executes a random back and forth motion. A homopolymer chain with N freely jointed segments of length L was considered by PT, which moves back and forth by one segment with a frequency ν.

The chain displaces down the tube in time in support of a number of segments, m. Here, is called the "diffusion coefficient" of m in one dimensional motion. The probability of the net displacement with m during time t in the range of $n - \Delta$ to $n - (\Delta + d\Delta)$ segments was calculated by PT. A Gaussian probability density was obtained for small times and large N. The total "crossing density" $\sigma(t)$ (chains per unit area) at junction surface then was calculated from the contributions of $\sigma_1(t)$ as a result of the chains still retain some portion of their initial tubes, plus a remainder, $\sigma_2(t)$. The $\sigma_2(t)$ contribution comes from the chains which have relaxed at least once.

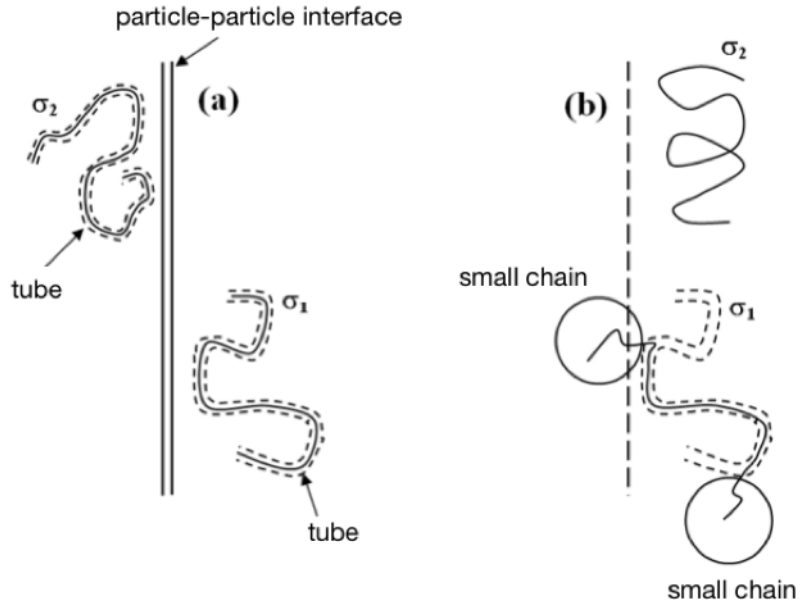

Figure 3.2 : A schematic representation of inter-diffusion during film formation process.

In terms of reduced time $\tau = 2vt/N^2$ the total crossing density can be written in the form of:

$$\frac{\sigma(\tau)}{\sigma(\infty)} = 2\pi^{-1/2}\left[\tau^{1/2} + 2\sum_{k=0}^{\infty}(-1)^n\left[\tau^{1/2}\exp\left(-\frac{k^2}{\tau}\right) - \pi^{-\frac{1}{2}}erfc(k/\tau^{1/2})\right]\right] \quad (3.7)$$

For small τ values, the summation term of the equation found above is very small and can be neglected, which then results in

$$\frac{\sigma(\tau)}{\sigma(\infty)} = 2\pi^{-1/2}\tau^{1/2} \quad (3.8)$$

This result was also predicted by de Gennes on the basis of scaling arguments [44]. At this point, it must be mentioned that the dependence on time, t in Equation 3.8 goes as $t^{1/4}$ at early times of the healing.

3.2 Percolation Theory

The basis of the percolation theory is to determine how a given set of sites, regularly or randomly positioned in some space, is interconnected [45]. At some critical probability, called the ‘‘percolation threshold (p_c)’’, a connected network of sites is formed that spans the sample, causing the system to percolate. In 1957, Broadbent and Hammersley [46], introduced the term ‘‘percolation theory’’ and used a geometrical

and statistical approach to solve the problem of fluid flow through a static medium. Initial work focused on the determination of the percolation thresholds in simple two- and three-dimensional geometries. Two types of percolation were considered: site percolation, where sites in a lattice are either filled or empty, or bond percolation, where all the sites in a lattice are occupied but are either connected or not [47]. Extensive simulations and theoretical work have shown that the percolation probability, $P_\infty(p)$ vanishes as a power-law near p_c:

$$\mathrm{P}_\infty(p) \approx (p - p_c)^\beta \tag{3.9}$$

For all volume fractions $p > p_c$, the probability of finding a spanning cluster extending from one side of the system to the other side is 1. The largest cluster spans the lattice connecting the left and right edges to the bottom edge, which is called ‘‘percolating cluster’’. Whereas for all volume fractions $p < p_c$, the probability of finding such an infinite clusters is 0. Percolation states in a lattice considering p_c is shown in the figure.

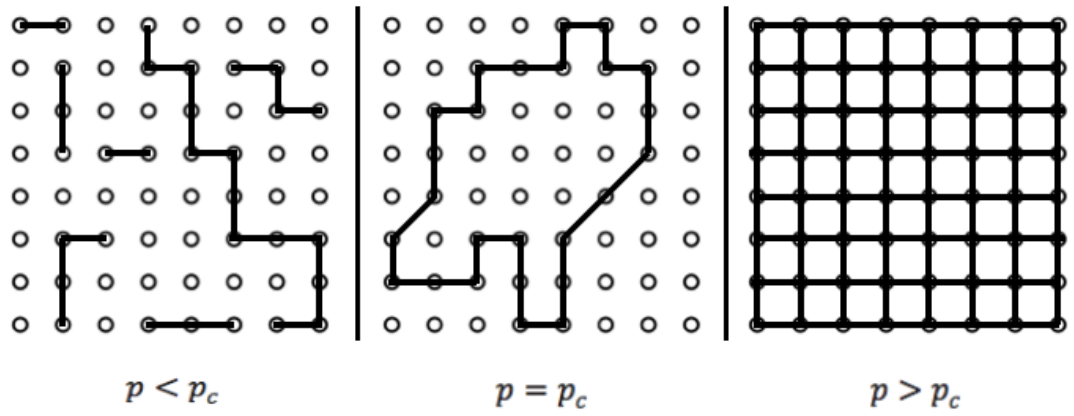

Figure 3.3 : A schematic representation of percolation in a square lattice. The small spots in a lattice represent the monomers.

Percolation theory has been employed to describe the electrical behavior of conducting and nonconducting circumstances of nanocomposite mixtures by considering the threshold mass fractions (percolation threshold, p_c) of the nanofillers. The abrupt transition from insulator to conductor is well clarified by percolation theory. The electrical conductivity of a composite is strongly dependent on the volume and/or mass fraction of the conductive phase. At low filler concentrations, the conductivity remains very close to the conductivity of the pure, electrically insulating polymer matrix since the fillers are dispersed individually or in small clusters in the matrix. A critical filler loading must be incorporated to transfer the composite from the insulator state into the

conductive state At this critical concentration, which is known as the percolation threshold, the electrical conductivity of the composite suddenly increases by several orders of magnitude. Often, at the percolation threshold, the filler forms a continuous network inside the polymer matrix, and increasing in the filler loading further usually has little effect on the composite electrical conductivity. Finally, the conductivity levels off at a certain value, the maximum conductivity of the composite. The conductivity, σ of a percolative system is generally described as a function of mass fraction, R by the scaling law in the vicinity of the percolation threshold (R_c):

$$\sigma = \sigma_0(R - R_c)^{\beta} \tag{3.10}$$

where σ is composite conductivity (in Siemens), σ_0 is the self-conductivity of MWCNTs film and is equal to 1. R present weight fraction of MWCNTs and R_c presents percolation threshold of conductivity. This equation is valid at concentrations above the percolation threshold ($R > R_c$). In this equation, the critical exponent β reflects dimensionality of the system and universality class of the problem [44]. For spherical particles in an insulating matrix, the theoretical random percolation value β is around 1.3 for a two-dimensional system and close to 2.0 for the three-dimensional system [45-48].

4. UV/VISIBLE SPECTROMETER

Photon transmission experiments and the optical analysis of prepared nanocomposite films containing polystyrene (PS) latex and nanofillers were performed by using UV-Visible spectrophotometer from Varian with a model number of Carry 100 bio UV-Visible (UVV). The transmitted light intensity, I_{tr}, of each film sample was measured at 550 nm where polystyrene, carbon nanotubes and graphene oxide do not have any specific absorption at this wavelength. Glass substrates which are truncated in the dimensions of 0.8x2.5 cm^2 were used as a standard for all UVV experiments. The experimental setup of the spectrophotometer that we used is given in figure to better understand how mechanism operates.

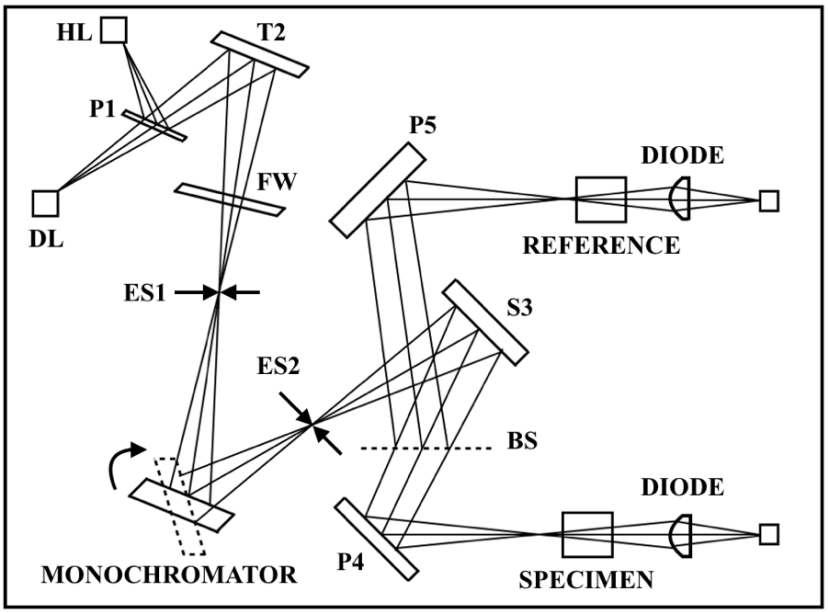

Figure 4.1 : Experimental Setup of Cary-100 UV Spectrophotometer.

The instrument has the slots of two quartz cuvettes in the measuring chamber where one of the slots is for reference while the other one refers to the specimen aimed to be measured. The light beam, has an intensity of I_0, of 1 cm height and 1 mm width reaches the photo-diodes through passing over the reference and the specimen. The intensity of light passing through the specimen, I_{tr}, can be followed up as a function

of wavelength and the collected data is simultaneously transferred to the computer which is attached to the spectrophotometer. The working interval of UV spectrophotometer that we used in our experiments is in the range between 190 nm and 1100 nm. Deuterium and halogen lamps are used as a light source in UV-spectrophotometer. Deuterium lamp is mostly used for the measurements in UV region in the range between 190 nm and 326 nm while halogen lamp is employed both for the measurements of visible and supraregional spectrum in the range between 326 nm and 1100 nm. Monochromator has a holographic concave grid of 1053 line/mm. The plane mirror, P1, can easily move with the help of a mechanical arm. When P1 is in the internal position, the light which comes from deuterium lamp (DL) is blocked and the light arise from the halogen lamp (HL) is reflected on a toroidal mirror, T2. The process of the source change at a specified wavelength occurs synchronously with the monochromator depending on the position of the P1 mirror. Monochromator constantly rotates around itself until the source change is over. The light beam which emerges from the source lamp focuses on the entry slot (ES1) by passing through the filter of FW while being reflected by T2 and it passes through ES1 to reach the monochromator. The light beam which focuses on the exit slot (ES2) reaches the spherical mirror, S3, by passing through the exit slot with the aid of monochromator. The light beam reflected from S3 is reflected on the beam splitter (BS). The BS reflects 50% of the light beam onto the planar mirror, P5 and the remaining 50% reaches the planar mirror, P4. The mirror P4 focuses the beam of light onto the sample which then it focuses on the specimen photodiode detector with the help of a simple convex lens. The mirror P5 focuses the light beam onto the reference cuvette and then the light beam is focused on the reference photodiode detector by the use of simple convex lens. The specimen which is aimed to be measured can contain more than one component such materials like nanocomposites. If a specific information about certain components of materials is needed, back correction process should be done by placing undesired material in the reference for the detection of their effect on the measurement. Since latex films cover the surface of glass substrates in the experiments, the light is not only affected by the film, however, also by the glass substrates. This means that the effect of glass should also be considered along with the change in the film. In this study, the baseline correction was conducted just before the measurements for working wavelength range in order to eliminate the errors. For this reason, the effect of glass on measurements was removed by considering the empty glass substrate as a reference.

5. EXPERIMENTAL PROCESS

5.1 Materials

5.1.1 Synthesis of polystyrene (PS) latexes

Polystyrene is one of the well-known and widely-used industrial polymers, particularly in the plastics industry. It is composed of branched styrene monomers as a result of a free radical vinyl polymerization process. In general, polystyrene is a thermoplastic class polymer in the solid form at the room temperature. However, they can be melted at higher temperatures while being processed by injection or extrusion processes. Polystyrene in a melted form can be solidified again with the cooling process. The density of polystyrene is about 1.05 g/ml in optimum conditions. Polystyrene is a versatile plastic that can be used either in the form of foams or rigid structures. They are mostly quite tough, fragile and bright. It is a cost-effective polymer with a relatively low melting point.

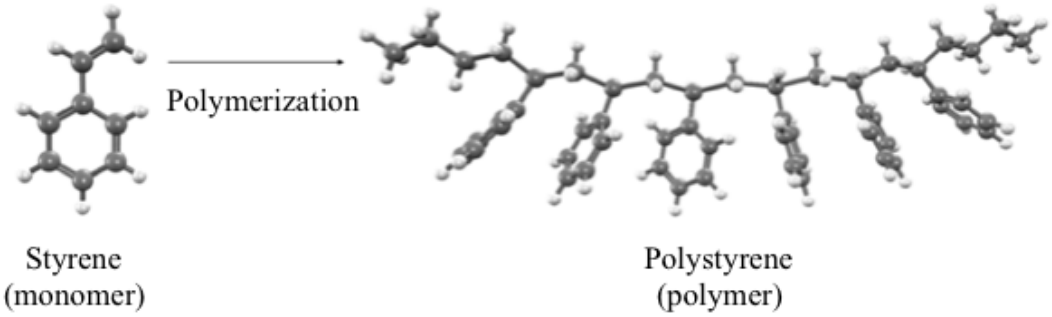

Figure 5.1 : Production of polystyrene from styrene monomers via polymerization process.

In this study, three types of polystyrene (PS) latex which have different diameters with same molecular weight were used to examine the effect of latex particle size on the film formation and electrical properties of PS/MWCNT nano-composites. PS latexes were synthesized by emulsion polymerization technique [49]. For each type of PS latex, the polymerization was performed batch-wisely using a thermostated reactor which is equipped with a condenser, thermocouple, mechanical stirring paddle and

nitrogen inlet. 50 ml of water, 3 g of styrene monomer (99% pure from Janssen) and the 0.014 g of fluorescent 1-Pyrenylmethyl methacrylate (PolyFluor® 394) were first mixed in the polymerization reactor where the temperature was kept constant at 70 °C. The water soluble radical initiator potassium persulfate (KPS) (1.6, 2 and 3% wt/wt, over styrene) dissolved in small amount of water (about 2 ml) was then introduced in order to induce styrene polymerization. As a surfactant, sodium dodecyl sulfate (SDS) at different concentrations (0.12, 0 and 0 % wt/vol) was added in the polymerization recipe to change the particle size keeping all other experimental conditions the same. The polymerization was conducted under 400 rpm agitation for 12 h under nitrogen atmosphere at 70 °C. The particle size was measured using Malven Instrument NanoZS based on light scattering measurement. Figure 5.2(a-c) presents SEM images of spherical PS particles with average particle sizes of 382 nm, 480 nm and 560 nm, respectively.

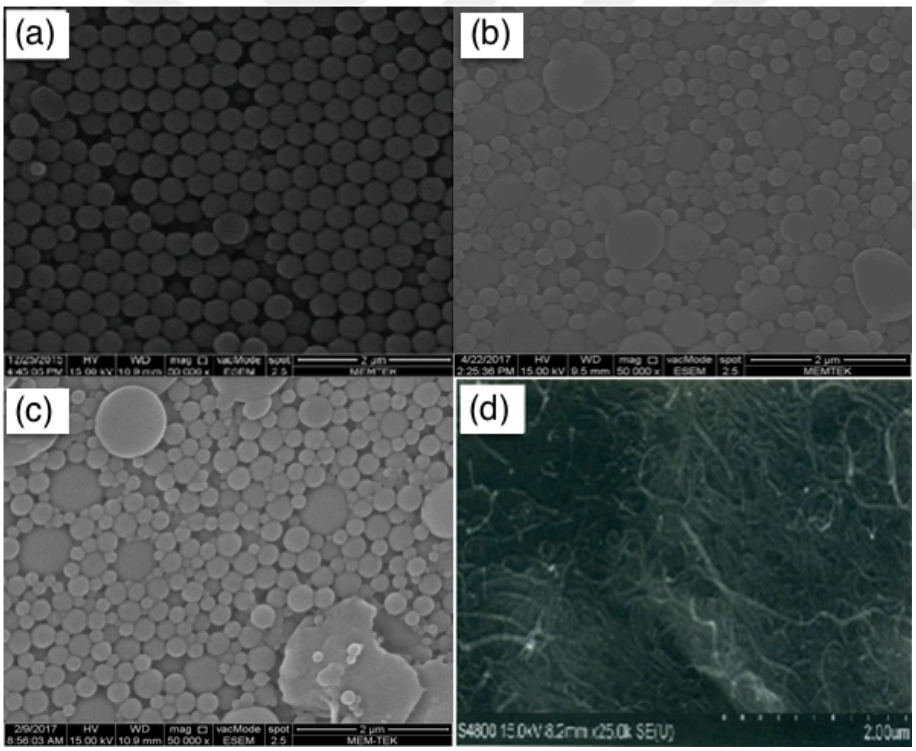

Figure 5.2 : SEM images of PS latexes with average particle sizes of (a) 382 nm, (b) 480 nm, (c) 560 nm and (d) MWCNTs used in this study.

The weight-average molecular weights (M_w) of individual PS chains (M_w) were measured by gel permeation chromatography (GPC) and found to be 98x10^3 g/mol in average. Glass transition temperature (T_g) of the PS latexes were determined using differential scanning calorimeter (DSC) and found to be around 105 °C. Table 5.1

provides some characteristics of the three parent latex dispersions used in preparation of the nanocomposite films.

Table 5.1 : Properties of the PS latexes.

PS latex size (nm)	Mw (10^3 g/mol)	T_g (°C)	SDS (wt/vol%)	kPS (wt%)
382	99.3	105	0.12	1.6
480	97.2	105	-	2.0
560	96.6	105	-	3.0

5.1.2 Multiwalled carbon nanotube (MWCNT) solutions

Multiwalled carbon nanotubes (MWCNTs) can be given as one of the foremost examples for the fabrication of electrically conductive nanocomposites. The rate of scientific studies in the field of nanoscience has dramatically increased as a result of remarkable properties of MWCNTs just after their discovery by Iijima [50]. Carbon nanotubes (CNTs) are essentially considered as the rolled graphene layers composed of numerous sp^2-hybridized carbon atoms in the form of cylindrical shape. Based on the number of nested rolled graphene sheets, CNTs can exist either as a singlewalled carbon nanotube (SWCNT) or multiwalled carbon nanotube (MWCNT). The electronic characteristics of SWCNTs are quite different when it is compared to MWCNTs. The significant characteristic of chirality which is directly associated with a regular arrangement of carbon atoms in a single wall endows either metallic or semi-metallic behavior to the MWCNTs. Furthermore, the CNTs with more than one single wall act as zero-gap metals, which indicates the importance of CNTs for the utilization as conductive nanofillers for future electronic applications [51]. Up to date, a number of research papers regarding electrical resistivity and electrical properties of multiwalled nanotubes (MWNTs) and singlewalled nanotube (SWNT) ropes have been reported [52]. One of the experimental research was done by Gojny indicates that the utilization of MWCNTs has a significant potential for the enhancement of electrical conductivity since MWCNTs have a greater dispersibility rather than SWCNTs [53]. Electrical conductivities of composite materials including CNTs as nanofillers are typically changing in the range between 10^{-5} and 10^{-2} S/m above the critical mass fraction of nanofiller which refers to percolation threshold [54]. The increment in volume fraction of MWCNTs can increase the electrical conductivity values of nanocomposite materials. According to previous studies in the literature, the overall resistance quantities of CNT-based composites and SWNT bundle networks are

prominently influenced by the contact resistances [55]. Since CNTs are under a strong effect of van der Waals forces, and possess a large surface area and a large aspect ratio, they are generally insoluble in various solvent medium and in the presence polymers. This circumstance can be the reason of formation of either aggregates or bundles which are tightly bound to each other [56,57]. Therefore, the difficulty in the dispersion of CNTs within polymer matrices as much as a need for higher inclusion of CNTs to promote percolative network formation is one can impede the development of CNT-based nanocomposites. However, the usage of surfactants and utilization of some special techniques such as ultrasonication can be the solution to cope with these difficulties.

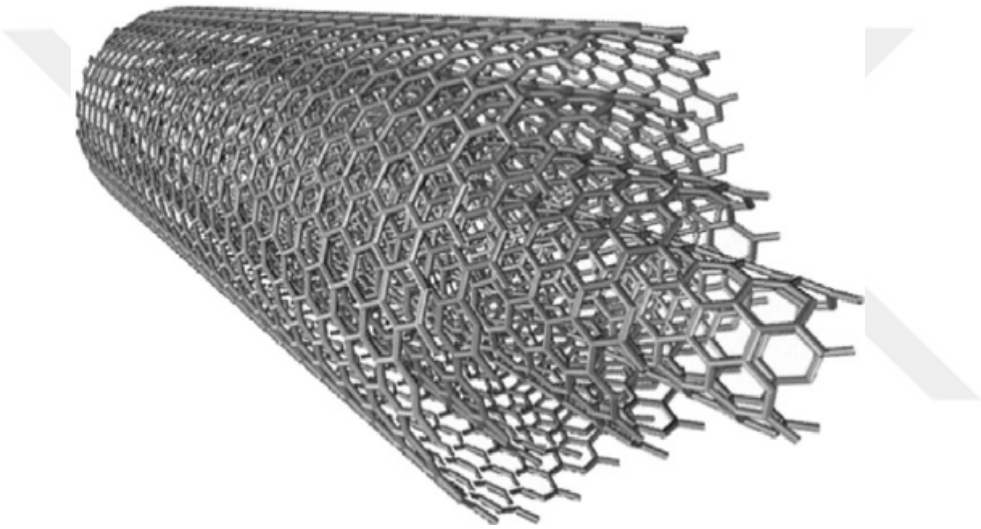

Figure 5.3 : A schematic representation of multiwalled carbon nanotubes (MWCNTs).

The MWCNTs used in this thesis work were purchased from Cheap Tubes Inc. (VT, USA), which were synthesized by split plasma technique. MWCNTs (length: 1–12 μm, outer diameter (OD): 13–18 nm, the density is approximately 2.1 g/cm^3, and purity is higher than 99 wt%) were used as supplied in black powder form without further purification. The MWCNTs are plasma purified and exfoliated, thus they can easily disperse in water. However, they still require the appropriate use of a surfactant and polyvinyl pyrolidone (PVP) is a good stabilizing agent for dispersions of carbon nanotubes, enabling preparation of nanocomposites from the dispersions of MWCNTs in PS solutions. A stock solution of MWCNTs (10 g/L) was prepared according to the manufacturer regulations as follows: nanotubes were dispersed in deionized (DI) water with the aid of PVP in the proportions of 10 parts of MWCNTs, 1–2 parts of PVP,

2.000 parts of DI water stirring for 3 h. Figures 5.2(d) and 5.3 [58] shows the SEM image of MWCNTs [59].

5.1.3 Graphene oxide (GO) solutions

Graphene and graphene-based materials have attracted an immense attention in the past several years due to their remarkable characteristics [60-63]. One of the most promising methods for large-scale production of graphene is strongly dependent on either the chemical or thermal reduction of graphene oxide (GO) which can cause undesired effects on the environment. As it is known that graphene sheets have a strong agglomeration tendency which considerably limits its application. Among numerous graphene-based materials, graphene oxide (GO) has great advantages as it is cost-effective, has an extraordinary structure, and is convenient for fabrication. Therefore, it has a great potential to be used as a reinforcing phase in composite materials.

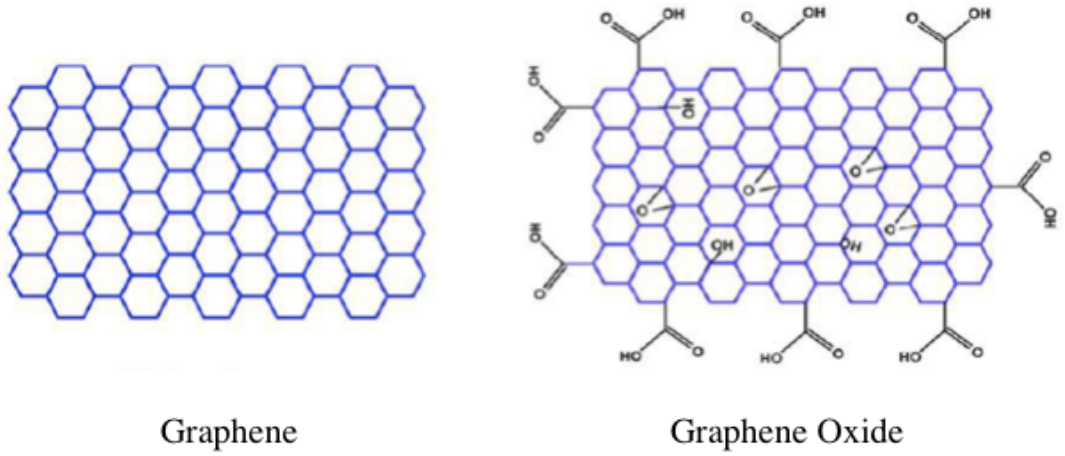

Figure 5.4 : A schematic representation of graphene and graphene oxide.

Graphene oxide (GO), is a single-atomic layered material composed of carbon, oxygen and hydrogen atoms, can be obtained by the treatment of graphite with powerful oxidizers [64]. In other words, GO can be defined as an oxidized form of graphene. The production of GO is easier than graphene layers. Their deposition as a coating material on substrates is fit especially for the fabrication of transparent conductive films since GO has a large surface area. The efficiency of oxidation process is strongly dependent on the carbon-oxygen ratio of GO. They are easily dispersed in the presence of water, organic solvents and such polymer matrices since GO has oxygen functionalities. The presence of oxygen groups is playing a significant role on the

dispersibility of GO within solvents. When the oxygen groups are removed, the reduced form of GO, called reduced graphene oxide, is more difficult for well-dispersion which results in the creation of aggregates. However, GO can be mixed with various polymers and other substances for the enhancement of properties of composite materials such as tensile strength, elasticity, electrical conductivity and so forth. GO flakes, in a solid state, attach from one to each other in order to form both thin and stable flat structures which can be folded and stretched. Thus, such GO structures can also be fit for applications such as hydrogen storage, ion conductors and nano-filtration membranes.

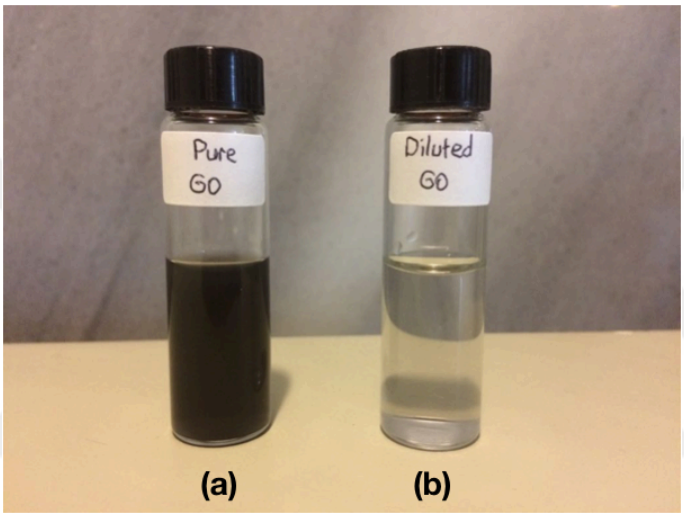

Figure 5.5 : Graphene oxide solutions (a) before and (b) after dilution process.

Commercial graphene oxide (GO), used throughout this study, were purchased from Sigma-Aldrich (Saint Louis, USA; 15-20 sheets; 4-10% edge-oxidized; dispersion in H_2O; sheet dimension variable; C:O ratio of the GO, as determined by EDX analysis, is close to one) as stable aqueous dispersions with a concentration of 1 mg/mL. GO dispersions were directly used without further purification. The original dark brown-colored GO suspension (see Figure 5.5(a)) was re-dispersed in distilled water to obtain aqueous GO suspension at a concentration of 0.5 mg/ml by a gentle sonication process. The resulting GO solution was then stirred for additional 2 h at the room temperature. Figure 5.5 shows the photograph of GO dispersion before and after dilution. The photo in Figure 5.5(b) shows that GO was readily exfoliated in water and neither sedimentation nor aggregation was noticed. The clear (or transparent) GO dispersion in Figure 5.5(b) clearly indicates the successful exfoliation driven by sonication combined with stirring.

5.2 Preparation of Nanocomposite Films

5.2.1 Preparation of PS/MWCNT nanocomposite films

For each type of PS particle, a 10 g/L stock solution of PS latex in water was prepared. The dispersion of MWCNTs in water was mixed with the solution of PS yielding the required ratio, R, of MWCNTs in PS latex by using the following relation

$$R\ (wt\%) = \frac{M_{MWCNT}}{M_{MWCNT} + M_{PS}} x100 \qquad (5.1)$$

where M_{PS} and M_{MWCNT} represent the weight of PS and MWCNTs in the mixture, respectively. Depending on the desired MWCNT concentration in the final nanocomposite mixture in the range from 0 wt% to 20 wt%, each dispersion of PS latex with different diameter were combined with the aqueous MWCNT-PVP solution under mechanical stirring, separately. The mechanical stirring was carried out at least for 1 h at the room temperature. The resulting composites were deposited as wet coating by placing the same number of drops on glass plates with similar surface areas which are about 0.8x2.5 cm^2 and allowing the water to evaporate at 45 °C in the oven. After drying process, the prepared samples were separately annealed above the glass transition temperature (T_g) of PS for 10 min at temperatures in the range from 100 to 250 °C. The temperature was maintained within ±2 °C during annealing. After each annealing step, films were removed from the oven and cooled down to the room temperature.

5.2.1 Preparation of PS/GO nanocomposite films

A homogeneous aqueous suspension of PS latex with a concentration of 0.5 mg/mL was firstly obtained under mechanical stirring. Then, prepared GO suspension above with a concentration of 0.5 mg/mL was mixed with PS latex suspension under magnetic stirring to obtain PS/GO suspensions with a ratio of GO to PS ranging from 0 to 100 wt%. These mixtures were then further sonicated for 2 h at room temperature for at least 3h to produce homogeneous mixtures. Glass slides with the dimensions of 0.8x2.5 cm^2 were used as substrates. The glass surface was firstly cleaned by the acetone and then cleaned sequentially with deionized water and finally dried in an oven. PS/GO solutions were drop-cast on the glass substrates and left to dry overnight at room temperature. We prepared a series of powder PS/GO composite films with

varying GO content from 0 wt% (PS only) to 100 wt%. In order to study the film-formation behavior of PS/GO composites, the produced films were separately annealed above T_g of PS, 105 °C for 10 min. at temperatures ranging from 100 °C to 250 °C. The samples were then cooled down to room temperature. The temperature was maintained within ±2 °C during annealing.

5.3 Measurements

5.3.1 Photon transmission measurements

Carry 100 bio UV–visible (UVV) spectrometer from Varian was used to take photon transmission measurements in our experiments. The transmittance values of the prepared PS/MWCNT nanocomposite films were detected at 550 nm while PS/GO nanocomposites were detected at 500 nm where the spectra of the nanocomposite are almost flat, i.e., polystyrene, multiwalled carbon nanotubes and graphene oxide have no specific absorption at this wavelength. A glass substrate was used as a standard for all UVV experiments.

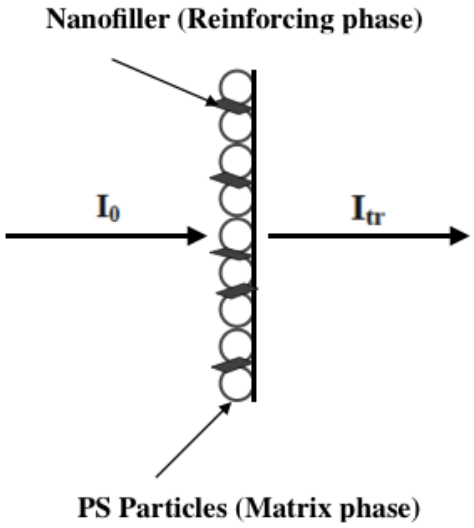

Figure 5.6 : A schematic illustration of glass substrate position.

5.3.2 Scanning electron microscope (SEM) measurements

Scanning electron micrographs (SEM) of the PS/MWCNT nanocomposite films were taken at 10–20 kV in a JEOL 6335F microscope. Micrographs of PS/GO nanocomposite films were taken at 10-20 kV by using scanning electron microscope

with a model of EVO LS 10 from Zeiss. For this purpose, a thin film of gold (10 nm) was sputtered onto the surface of the prepared samples by the help of a Hummer-600 sputtering system to assist image the PS/MWCNT and PS/GO nanocomposite films against the glass background.

5.3.3 Electrical conductivity measurements

The electrical conductivity of all PS/MWCNT and PS/GO nanocomposite films was measured by a two-probe method through using a Keithley Model 6517a Electrometer with an ultrahigh resistance meter. For the surface resistance measurements, the samples were coated onto thin rectangular glass slabs with typical dimensions of 2.5x2.5 cm^2.

The electrical contact was made by using a silver paste. Electrical resistivities of the nanocomposite films were measured by alternating polarity technique with electrometer and a test fixture.

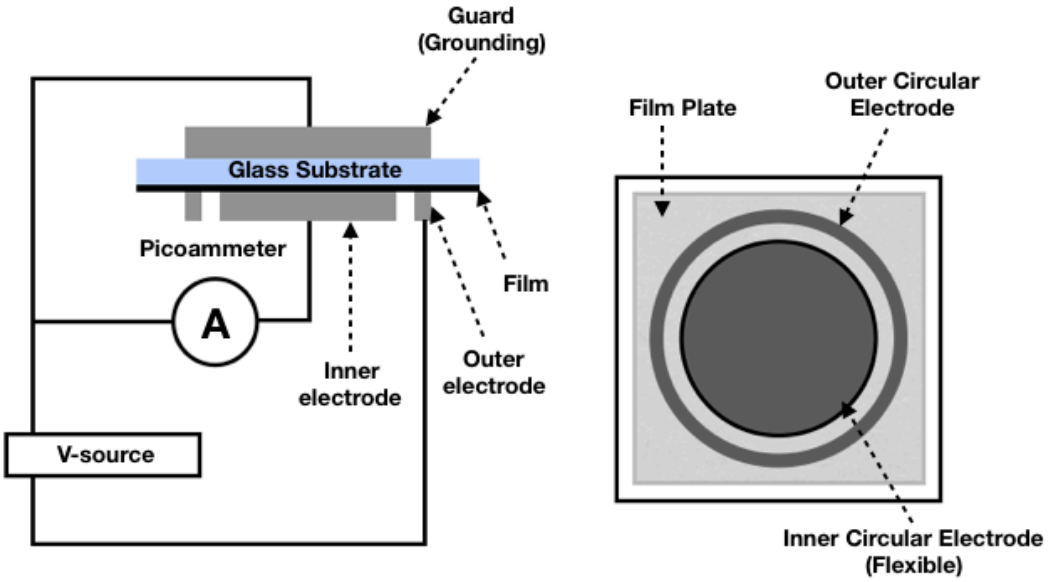

Figure 5.7 : Experimental setup of Keithley Model 6517a Electrometer with an ultrahigh resistance meter.

The nanocomposite films were placed in the text fixture, which have disk shaped electrodes, then their surface resistivities, $R_s(\Omega)$, were measured for 15 s under 100 V alternating potential.

All the resistivity values of the nanocomposite films were determined for four different orientations and measurements were repeated many times to lower the error

percentage. The surface resistivity was converted into surface conductivity by using the following relationship $\sigma = 1/R_s$ where σ is the electrical conductivity. Experimental setup [65] is given in Figure 5.7.

6. RESULTS AND DISCUSSION

6.1 PS/MWCNT Nanocomposite Films

6.1.1 Film formation process of PS/MWCNT nanocomposite films

Transmitted light intensities, I_{tr}, versus annealing temperatures are plotted in Figures 6.1 - 6.3 for the films including 0, 1.0, 1.5, 3.5, 7.5 and 10 wt% of MWCNT content of the nanocomposites which are made up of 382 nm, 480 nm and 560 nm of PS particles, respectively.

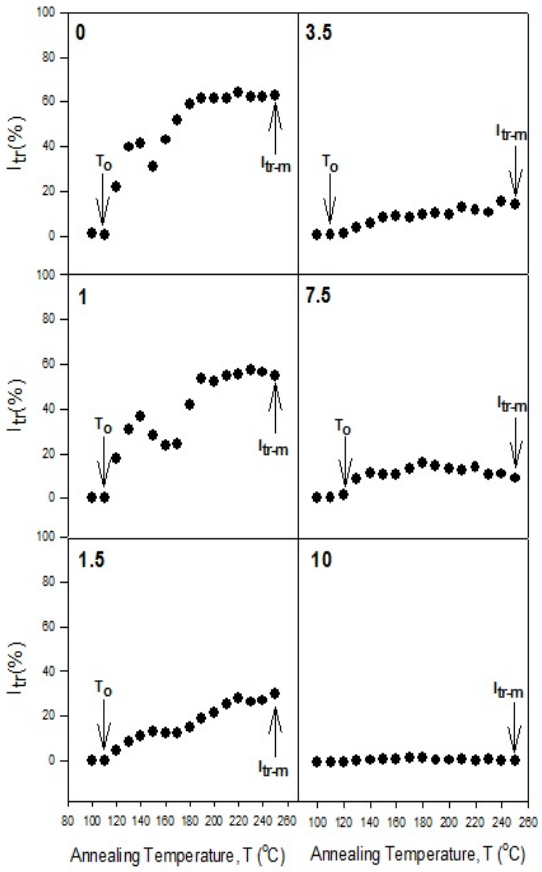

Figure 6.1 : Plots of transmitted photon intensities, I_{tr}, vs. annealing temperatures depending on MWCNT content in the films for the nanocomposite system made from 382 nm latex particle. The numbers on each figure show the MWCNT content in the film. T_0 is the minimum film formation temperature.

Upon annealing, the transmitted light intensity, I_{tr}, started to increase above a certain onset temperature, called the minimum film-formation temperature T_0, for the film samples in the range between 0 wt% and 7.5 wt% of MWCNT for 382 nm of PS latex and in the range between 0 wt% and 5 wt% of MWCNT for 480 nm and 560 nm of PS latex. The increase in I_{tr} with annealing can be explained by the evaluation of the transparency of the films and surface smoothing upon annealing.

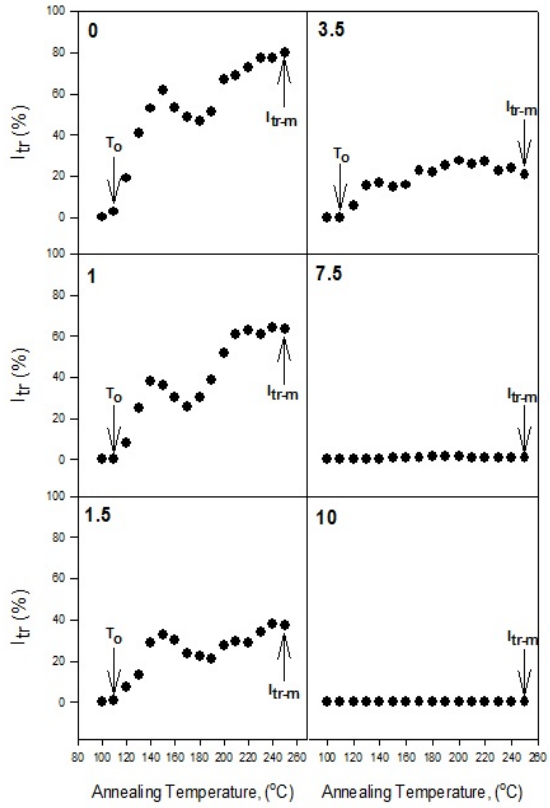

Figure 6.2 : Plots of transmitted photon intensities, I_{tr}, vs. annealing temperatures depending on MWCNT content in the films for the nanocomposite system made from 480 nm latex particle.

Most probably, the increase in I_{tr} above T_0 up to healing temperature (T_h) (see Figures 6.4 – 6.6) corresponds to the void closure process [66] i.e., the polystyrene starts to flow upon annealing and voids between particles can be filled. On the other hand, the increase in I_{tr} above T_h corresponds to the interdiffusion process. However, above this range, I_{tr} is almost zero and does not change with annealing, which indicates that light transmission is completely blocked by the dispersion of the MWCNTs in the nanocomposite films. On the other hand, I_{tr} decreases with increasing MWCNT content in the films at all annealing temperatures, predicting that less transparency occurs in the films which have the high percent of MWCNTs due to the light scattering.

The maximum values of $(I_{tr})_m$ for all film series in Figures 6.1 – 6.3 confirm this picture i.e., as the MWCNT content is increased, $(I_{tr})_m$ decreases continuously to its minimum value of 0% around 10 wt% of MWCNT for the composite system made from 382 nm PS latex and 7.5 wt% of MWCNT for 480 nm and 560 nm of PS latexes.

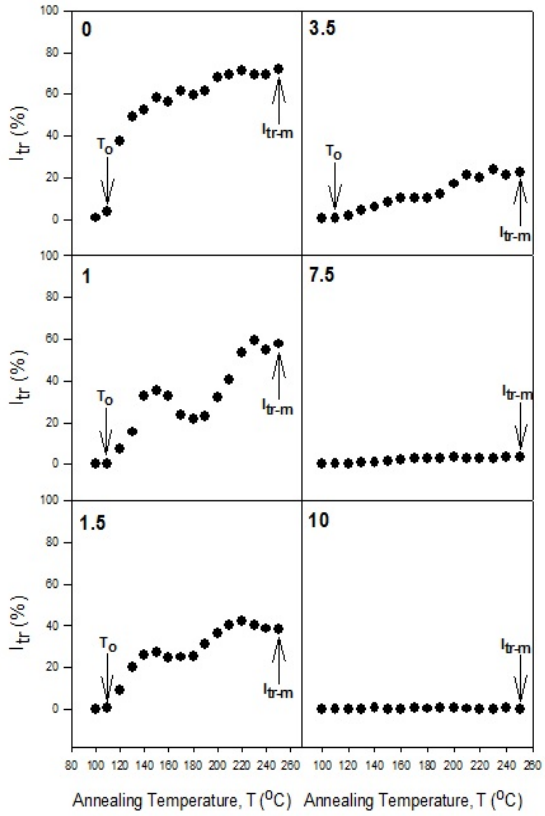

Figure 6.3 : Plots of transmitted photon intensities, I_{tr}, vs. annealing temperatures depending on MWCNT content in the films for the nanocomposite system made from 560 nm latex particle.

Minimum film formation (T_0) and healing (T_h) temperatures are important characteristics related to the film-formation properties of latexes. The T_0 and T_h values were measured for all nanocomposite film series and reported in Table 6.1. T_0 is often used to indicate the lowest possible temperature for particle deformation which is sufficient to decrease interstitial void diameters to sizes well below the wavelength of light [67]. Below this critical temperature, the dry latex is opaque and powdery. However, at and/or above this temperature, a latex cast film becomes continuous and clear film [68]. Therefore, T_0 has been considered in this study as the temperature above where the I_{tr} starts to increase. The healing temperature (T_h) is the minimum temperature in which the latex film becomes continuous and free of voids. The healing point indicates the onset of the particle–particle adhesion [68]. Here, T_h is defined as

the intersection of of two broken lines from the logaritmic plot of I_{tr} curves versus temperature (see Figures 6.4 – 6.6).

Table 6.1 : T_0 (°C) and T_h (°C) temperatures for three PS/MWCNT nanocomposite film systems.

MWCNT Content (wt%)	PS latex (382 nm)		PS latex (480 nm)		PS latex (560 nm)	
	T_0 (°C)	T_h (°C)	T_0 (°C)	T_h (°C)	T_0 (°C)	T_h (°C)
0.0	110	130	110	150	110	120
0.5	110	140	110	130	110	140
0.75	110	130	110	140	110	140
1.0	110	130	110	140	110	140
1.5	110	130	110	140	110	140
2.5	110	140	110	130	110	150
3.5	110	140	110	130	110	130
5.0	110	130	110	130	110	170
7.5	120	130	-	-	-	-

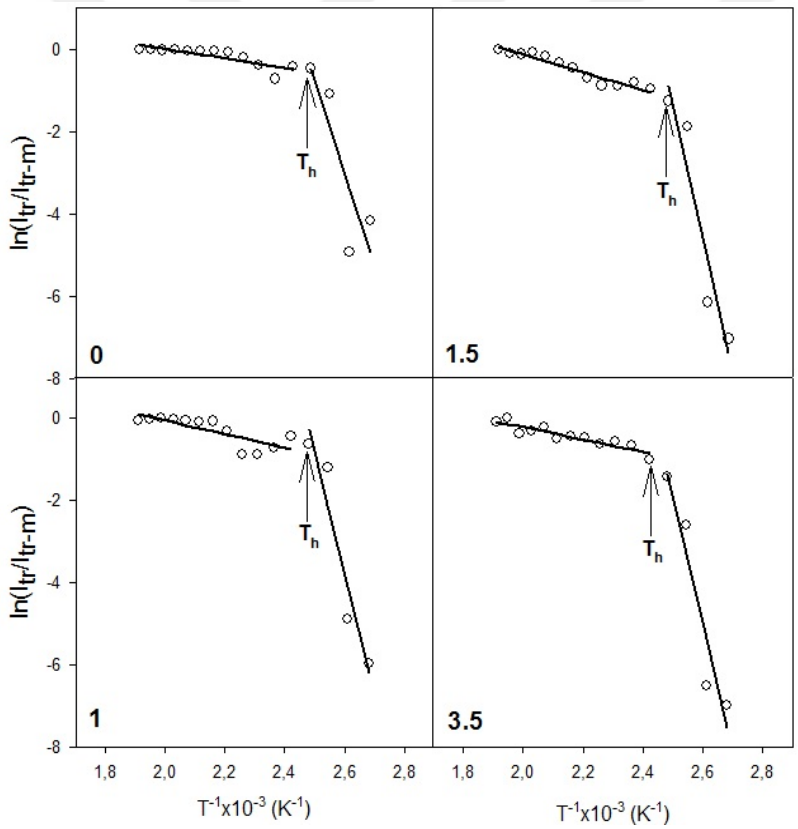

Figure 6.4 : The $\ln(I_{tr})$ vs. T^{-1} plots of the data in Figure 6.1. The slope of the straight lines produces ΔH and ΔE activation energies, which are listed in Table 6.2.

From Table 6.1, it is seen that T_0 and T_h do not change so much within each film set indicating that film formation of PS latexes are not affected with MWCNT content in the films. In addition, as shown in Table 6.1, the T_0 values do not change with particle

size of PS latexes. However, T_h values are shifted to higher temperatures with the increase in PS latex particle size where 130 °C - 140 °C for 382 nm, 130 °C - 150 °C for 480 nm and 120 °C - 170 °C for 560 nm of PS latex.

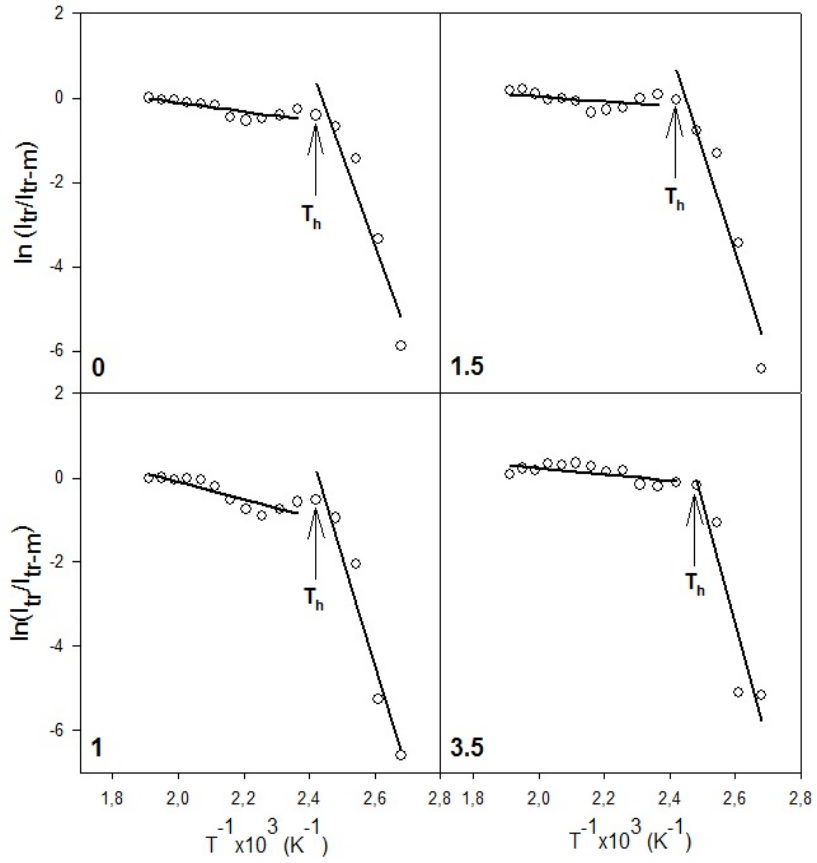

Figure 6.5 : The $\ln(I_{tr})$ vs. T^{-1} plots of the data in Figure 6.2. The slope of the straight lines produces ΔH and ΔE activation energies, which are listed in Table 6.2.

This result points out that film formation by PS latex polymers is strongly influenced by the latex size and shifted to higher temperature region with increasing of particle size. In order to quantify the behavior of I_{tr} curves below T_h presented in figures 6.4 and 6.6, the model of void closure can be implemented, where decrease in void size (r) leads to the increase in the ratio of $I_{tr}/(I_{tr})_m$ and vice versa. If the assumption is made that the ratio of $I_{tr}/(I_{tr})_m$ is inversely proportional to the 6th power of void radius, r then Equation 3.6 can be written as:

$$t = \frac{2AC}{\gamma} exp\left(\frac{\Delta H}{kT}\right)\left(\frac{I_{tr}}{(I_{tr})_m}\right)^{1/3} \qquad (6.1)$$

where r_0^{-2} is omitted from the relation as it is quite small when it is compared to r^{-2} values after a void closure process is initiated.

The Equation 6.1 found above can be solved for $I_{tr}/(I_{tr}\,)_m$ in the form of:

$$I_{tr}(T) = S(t)exp\left(-\frac{3\Delta H}{kT}\right) \tag{6.2}$$

where $S(t) = (\gamma t/2AC)^3$, and $I_{tr}/(I_{tr}\,)_m$. For a given time, the logarithmic form of Equation 6.2 can be written as follows:

$$\ln\big(I_{tr}(T)\big) = \ln\big(S(t)\big) - \left(\frac{3\Delta H}{k_B T}\right) \tag{6.3}$$

The increase in I_{tr} intensity below and above the T_h point (see Figures 6.4 – 6.6) can be explained by the void closure and interdiffusion processes, respectively [69]. Equation 6.3 can now be used to produce viscous flow activation energies, ΔH. $\ln(I_{tr})$ versus T^{-1} plots and their fits to Equation 6.3 are presented in the Figures 6.4 – 6.6 (right hand side of the curves) from which ΔH activation energies were obtained.

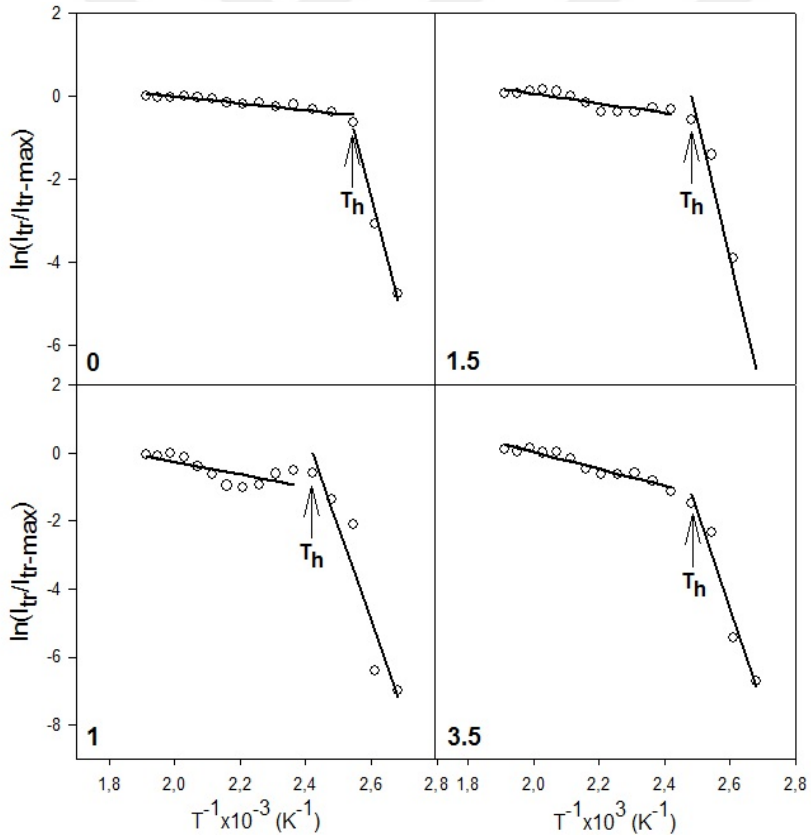

Figure 6.6 : The $\ln(I_{tr})$ vs. T^{-1} plots of the data in Figure 6.3. The slope of the straight lines produces ΔH and ΔE activation energies, which are listed in Table 6.2.

The measured void closure, ΔH activation energies are listed in Table 6.2. It is seen that energy values do not change much with increasing of MWCNT content for each

nanocomposite film system, i.e. the amount of heat which was required by one mole of polymeric material to accomplish a jump during viscous flow do not change by varying the MWCNT content. From here, it is understood that energy need for viscous flow for PS particles is not affected by the MWCNT content.

Since MWCNTs subside in PS matrix as bundles, they do not affect the void closure process. The average values of ΔH were calculated as 10 kcal/mol, 18 kcal/mol and 19 kcal/mol for the nanocomposite films made from 382 nm, 480 nm and 560 nm of PS particles, respectively.

Table 6.2 : Experimentally produced void closure (ΔH) and interdiffusion (ΔE) activation energies.

MWCNT Content (wt%)	PS latex (382 nm)		PS latex (480 nm)		PS latex (560 nm)	
	ΔH kcal.mol^{-1}	ΔE kcal.mol^{-1}	ΔH kcal.mol^{-1}	ΔE kcal.mol^{-1}	ΔH kcal.mol^{-1}	ΔE kcal.mol^{-1}
0.00	14.8	4.40	14.1	4.2	20.0	3.20
0.50	5.10	3.40	22.1	4.6	18.6	3.20
0.75	14.6	5.90	13.4	6.7	17.9	7.20
1.00	19.6	4.50	16.8	8.2	18.3	7.50
1.50	21.5	8.80	17.7	2.6	21.4	4.50
2.50	11.8	5.20	21.1	3.3	19.8	4.80
3.50	17.4	6.00	20.5	3.3	20.5	10.8
5.00	21.2	10.6	18.7	0.4	15.3	10.8
7.50	26.0	7.30	-	-	-	-
Av.	**16.88**	**6.23**	**18.05**	**4.16**	**18.98**	**6.5**

From these values, it is seen that ΔH values increase with increasing PS latex size. This implies that the viscous flow process is mostly affected by the PS particle size.

The PS particles with smaller diameters have larger surface area or surface free energy. As their total surface energy is much less than that of small PS particles, larger PS particles require higher energy to complete the viscous flow process.

For the comparison of our results with the crossing density of the PT model, the temperature dependence of $\sigma(\tau)/\sigma(\infty)$ can be modeled by taking Arrhenius relation into consideration for the linear diffusion coefficient as follows:

$$\nu = \nu_0 \exp\left(-\frac{\Delta E_b}{kT}\right) \tag{6.4}$$

where ΔE_b is defined as the activation energy for backbone motion of polymers depending on the temperature interval. By the combination of Equation 3.8 and 6.4, a useful relation can be expressed as

$$\frac{\sigma(\tau)}{\sigma(\infty)} = A_0 \exp\left(-\frac{\Delta E_b}{2kT}\right) \tag{6.5}$$

where $A_0 = (8\nu_0 t/\pi N^2)^{1/2}$ is a coefficient which is independent of temperature. The increase in I_{tr} above T_h is already related to the vanishing of particle-particle interfaces i.e. since annealing temperature is increased, much more chains are getting relaxed across the junction surface which results in the increase in crossing density. Now, it can be considered that I_{tr} is proportional to the crossing density $\sigma(t)$ in Equation 6.5 and then the phenomenological equation can be given as follows

$$\frac{I_{tr}(\mathrm{T})}{I_{tr}(\infty)} = \mathrm{Aexp}\left(-\frac{\Delta \mathrm{E}}{2\mathrm{kT}}\right) \tag{6.6}$$

Logarithmic plots of I_{tr} vs. T^{-1} are presented in the Figures 6.4 – 6.6 (left hand side of the curves) for various MWCNT content. The activation energies, ΔE are produced by least squares fitting the data to equation 16 and are listed in Table 6.2, where it is seen that ΔE values do not change much with increasing MWCNT for 382 nm and 480 nm particle sizes indicating that MWCNT content does not affect the backbone motion of the polymer chains across the junction surfaces in these films.

The calculated activation energies were found roughly independent of MWCNT content in the film, since the film formation occurred on top surface of composites during annealing. However, the ΔE value of 560 nm particles increases with increasing MWCNT indicating that much energy is required to accomplish the interdiffusion process across the junction surface at high MWCNT content for this composite system. When the MWCNT content is increased, some PS particles in this composite system are wrapped by MWCNTs (see Figure 6.11) and the average number of contacts between PS particles is prevented in some part of the film.

As a result, in the case of increasing MWCNT content, the interpenetration of PS chains requires higher energy to accomplish their motion due to the physical restrictions by MWCNT particles for 560 nm latex system. This result is in consistent with the behavior of T_h with increasing PS size.

Furthermore, the average values of ΔE were calculated as 6.2 kcal/mol, 4.2 kcal/mol and 6.5 kcal/mol for composites prepared from 382 nm, 480 nm and 560 nm PS particles, respectively. This indicates that ΔE values are not affected by particle size.

6.1.2 Film morphology of PS/MWCNT nanocomposite Films

In order to gain more information about the organization of MWCNTs in the PS matrix for three nanocomposite systems during annealing, the SEM and FE-SEM images of the PS/MWCNT nanocomposites containing 0, 2.5 and 10 wt% of MWCNT content annealed at 100 °C and 250 °C compared in the Figures 6.7 – 6.10 and in the Figures 6.11 – 6.13, respectively.

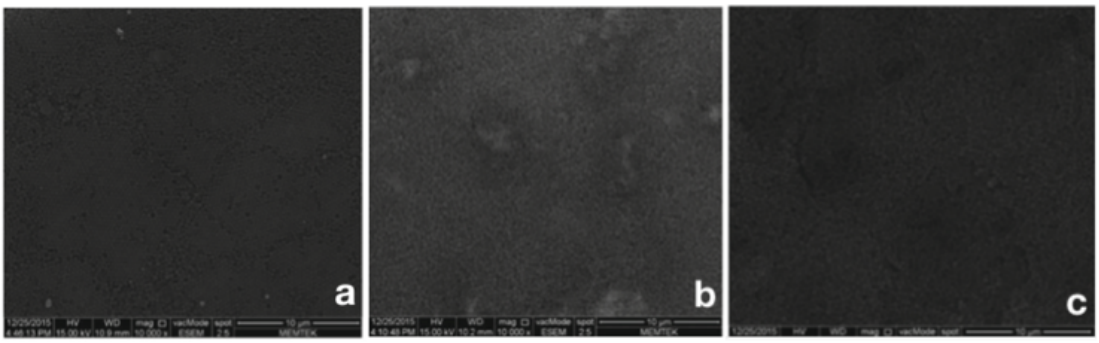

Figure 6.7 : SEM images of 382 nm nanocomposite system for (a) 0, (b) 2.5 and (c) 10 wt% MWCNT content films annealed at 100 °C for 10 min.

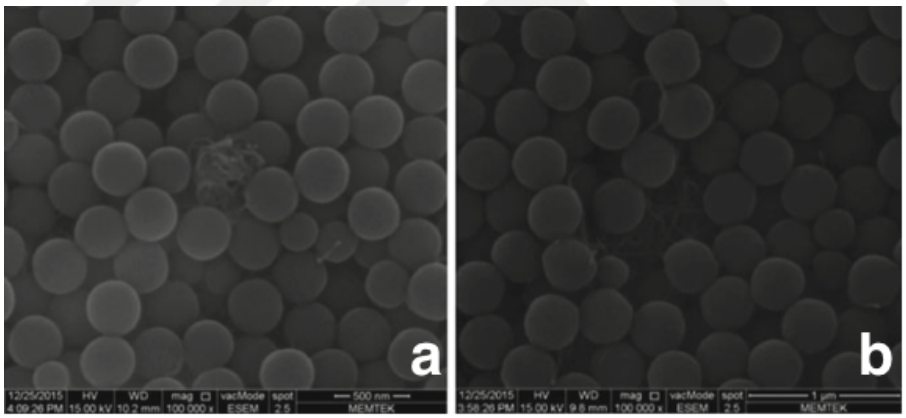

Figure 6.8 : FE-SEM images of 382 nm nanocomposite system taken in higher magnification (x100 000) for (a) 2.5 and (b) 10 wt% MWCNT content films annealed at 100 °C for 10 min. MWCNT bundles are clearly seen in these films.

After annealing the composite films at 100 °C (see Figures 6.7 – 6.10), no deformation in PS particles is observed and PS particles keep their original spherical shapes for all nanocomposite films. However, in nanocomposite system which is made up of 382 nm of PS particles (see Figure 6.8), for 2.5 and 10 wt% of MWCNT content some depressions are seen in these films. In order to understand these depressions, the higher magnification images of these films were taken and given in Figure 6.8. From these images, it is understood that these depressions are due to the MWCNT bundles which

are subsided in PS powder films. When the latex/MWCNT mixture was coated on the substrate and was dried, the MWCNTs would subside to the bottom layer during the evaporation of water due to their high density for this nanocomposite system.

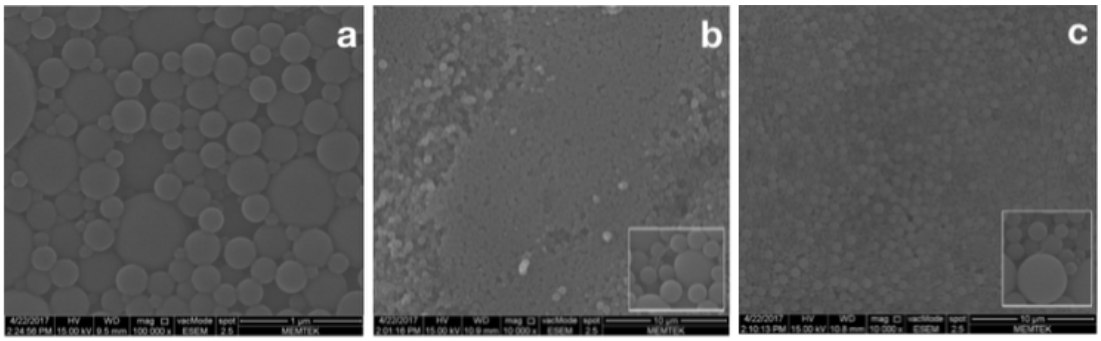

Figure 6.9 : FE-SEM images of 480 nm nanocomposite system for (a) 0, (b) 2.5 and (c) 10 wt% MWCNT content films annealed at 100 °C for 10 min.

However, almost no such depressions are seen for the nanocomposites prepared from 480 nm and 560 nm of PS particles in the Figures 6.9 and 6.10. It is observed that some PS particles in these PS/MWCNT nanocomposite powder films were wrapped by MWCNTs or were connected by MWCNT bundles. These regions are indicated by the white arrows and illustrated in enlarged image (insets of Figures). It is also seen that some nanotubes are stretched out across the PS particles. Compared to the other morphological states which are shown in the Figure 6.7(b-c), the PS/MWCNT nanocomposites in Figures 6.9(b-c) and 6.10(b-c) show relatively better dispersion.

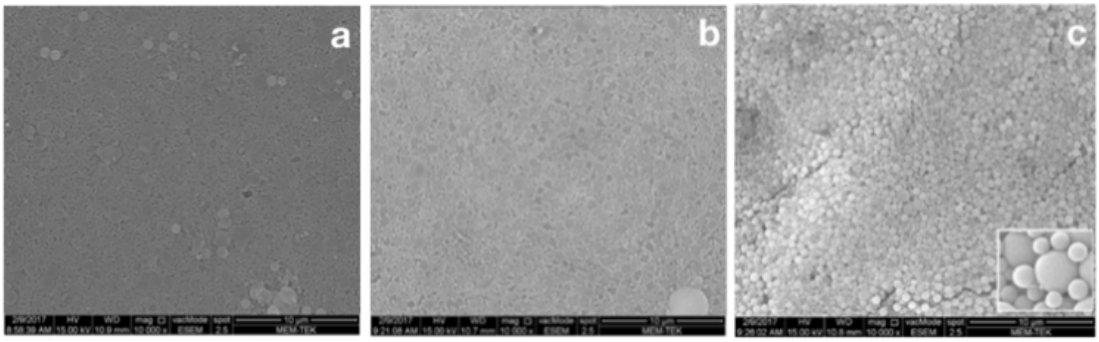

Figure 6.10 : FE-SEM images of 560 nm nanocomposite system for (a) 0, (b) 2.5 and (c) 10 wt% MWCNT content films annealed at 100 °C for 10 min.

Thus, it is believed from these morphological image that the distribution of MWCNTs in PS matrix is maintained more uniformly by increasing PS particle size. After annealing treatment at 250 °C (see Figures 6.11 – 6.13), SEM and FE-SEM images

show that complete particle coalescence has been achieved in all nanocomposite systems.

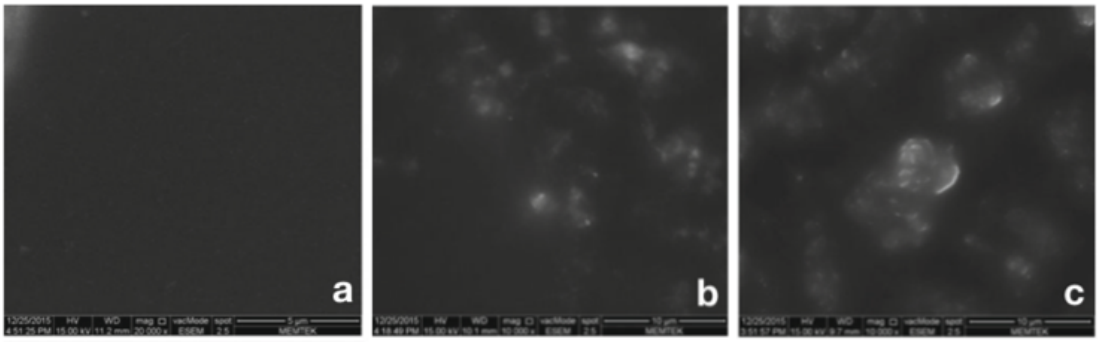

Figure 6.11 : SEM images of 382 nm nanocomposite system for (a) 0, (b) 2.5 and (c) 10 wt% MWCNT content films annealed at 250 °C for 10 min.

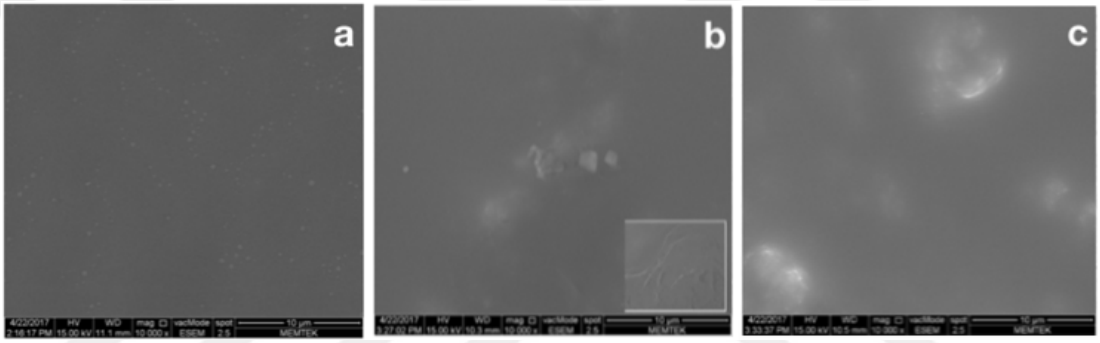

Figure 6.12 : SEM images of 480 nm nanocomposite system for (a) 0, (b) 2.5 and (c) 10 wt% MWCNT content films annealed at 250 °C for 10 min.

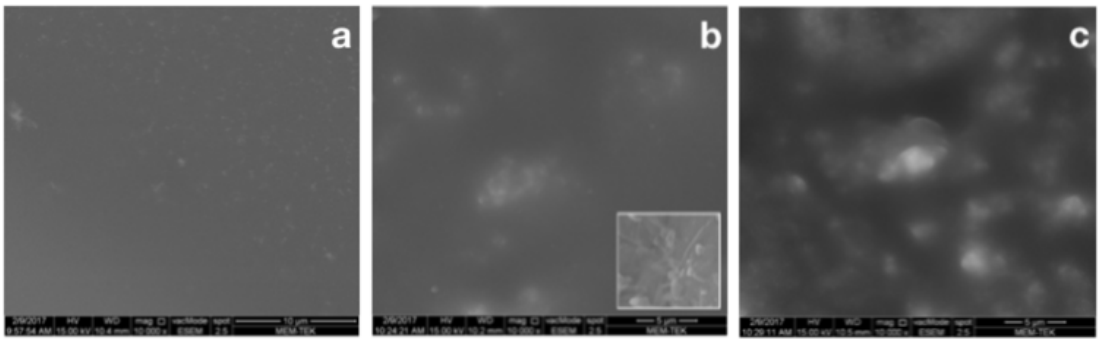

Figure 6.13 : SEM images of 560 nm nanocomposite system for (a) 0, (b) 2.5 and (c) 10 wt% MWCNT content films annealed at 250 °C for 10 min.

It is seen that all memory of the original particles is lost and a continuous latex film formed due to the interdiffusion of polymer chains. SEM and FE-SEM images of pure PS (0 wt% of MWCNT) film surfaces in the Figures 6.11(a), 6.12(a) and 6.13(a) appear relatively smooth and flat, revealing that a continuous and homogenous film is formed.The Figures 6.11(b), 6.12(b) and 6.13(b) show SEM and FE-SEM images of

the surfaces of PS/MWCNT nanocomposite films for three different nanocomposite systems with 2.5 wt% of MWCNT content. Here the bright areas represent conductive MWCNT bundles in the insulating PS polymer matrix. These small and large MWCNT bundles are seen to disperse in the PS network with very few contacts between each other in the films. Some of them just lay close to each other without contacting each other. However, the size and the number of contacts between the MWCNT bundles increased with increasing of MWCNT content (Figures 6.11(c) and 6.13(c)) forming a continuous conductive network in the polymer matrix. Here, due to annealing at 250 °C, PS particles deformed and they became a continuous phase in the top layer and played an essential role in the connection of conductive MWCNTs bundles in the bottom layer. As a result, a conductive network was constructed after the film-forming process. In addition, these bundles also cause strong light scattering resulting in low I_{tr} values which confirm the optical transmission results given in the Figures 6.1 – 6.3. The morphology of the surface of the nanocomposite films with 10 wt% of MWCNT content made up of 480 nm and 560 nm PS Show less surface regularity compared to 382 nm PS latex system. These films seen flatter in shape indicating that tightly entangled MWCNT bundles changed into the loosely entangled clusters in these films. In other words, in these two nanocomposites systems, the cluster like morphology is seen slightly to change into the uniform morphology of the nanocomposites. Namely, some of the MWCNTs are individually dispersed in PS polymer matrix (see insets of Figures 6.9 and 6.10).

6.1.3 Electrical conductivity and electrical percolation behavior of PS/MWCNT nanocomposite films

Figure 6.14 shows the effect of MWCNT concentration on the electrical conductivity (σ) of three PS/MWCNT composite film systems as a function of MWCNT content annealed at 250 °C. The surface conductivity properties of the films were measured at room temperature by using a two probe technique. As the MWCNT content was in the range of (0-1.5) wt%, a substantially low surface conductivity was obtained (10^{-15}-10^{-14} S for 382 nm system, 10^{-13}-10^{-12} for 480 nm system and 10^{-13}-10^{-11} S for 560 nm system), typical of dielectric materials, because of insufficient connection of the conductive network. All nanocomposite system exhibit a significant conductivity enhancement at R_c=1.5 wt%, indicating the formation of a percolating MWCNT network. The electrical conductivity of composites abruptly increases by many orders

of magnitude when the filler content, R exceeds the threshold concentration, R_c. The conductivity of pure PS films is in the order of 10^{-15}-10^{-13} S, and for an MWCNT concentration of 2.5 wt% conductivity of $1.1\text{x}10^{-10}$ S for 382 nm, $1.9\text{x}10^{-8}$ S for 480 nm and $3.9\text{x}10^{-8}$ S for 560 nm can be achieved. Following the initial formation of the conductive network, adding more MWCNTs results in a further increase in the conductivity.

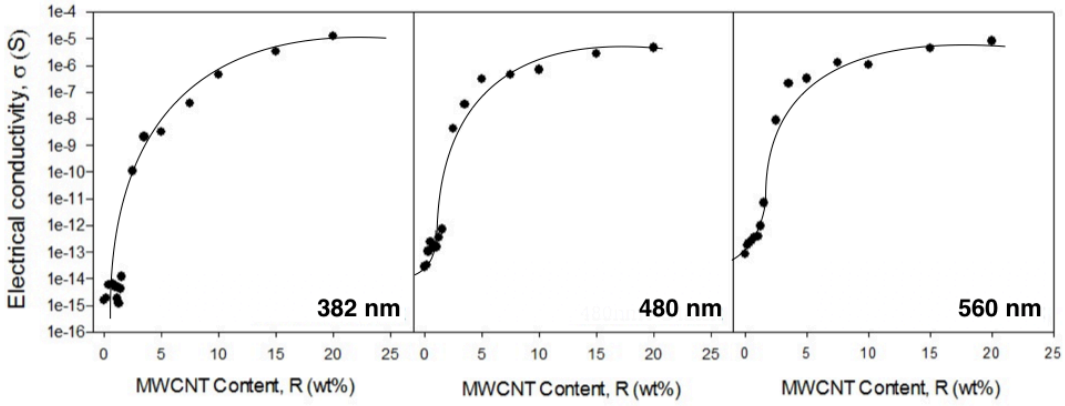

Figure 6.14 : Conductivities, σ, and their best fitted curves of PS/MWCNTs nanocomposites for different PS particle sizes as a function of MWCNT content, R (wt%).

When the content of MWCNT was 20 wt%, the conductivity reached 10^{-5} S for 382 nm and 480 nm, 10^{-4} S for 560 nm particle systems, respectively. This shows that the incorporation of MWCNT increased the conductivity by 9-10 orders of magnitude, from 10^{-15}-10^{-13} S for the pure PS polymers to 10^{-5}-10^{-4} S at 20 wt% MWCNTs. As a result of introducing more MWCNTs into the system, above 1.5 wt%, significant alterations to the structure occurred.

Owing to the large bundle diameter and higher MWCNT content, disorder in the latex structure is induced as shown in the Figures 6.11 – 6.13. Here, it is seen that the increase of PS latex size enhanced the electrical conductivity and increased the conductivity one order of magnitude from 10^{-5} S (for 382 nm and 480 nm latex systems) to 10^{-4} S (for 560 nm latex system). In order to calculate the percolation threshold, Equation 3.10 was transformed into the logarithmic form:

$$\log(\sigma) = \log(\sigma_0) + \beta log|R - R_c| \tag{6.7}$$

Then to produce an estimated value for R_c, and the critical exponent, β we fitted the $\log(\sigma)$-$log|R - R_c|$ data in Figure 6.15 for $R > R_c$, to Equation 6.7. Here, due to the limitation on getting more data in critical region, we used the continuous function fitted

best to the experimental points in Figure 6.14. The value of β has been determined from the slope of the linear relation of $\log(\sigma)$-$log|R - R_c|$ plot of the best fitted curve in Figure 6.15.

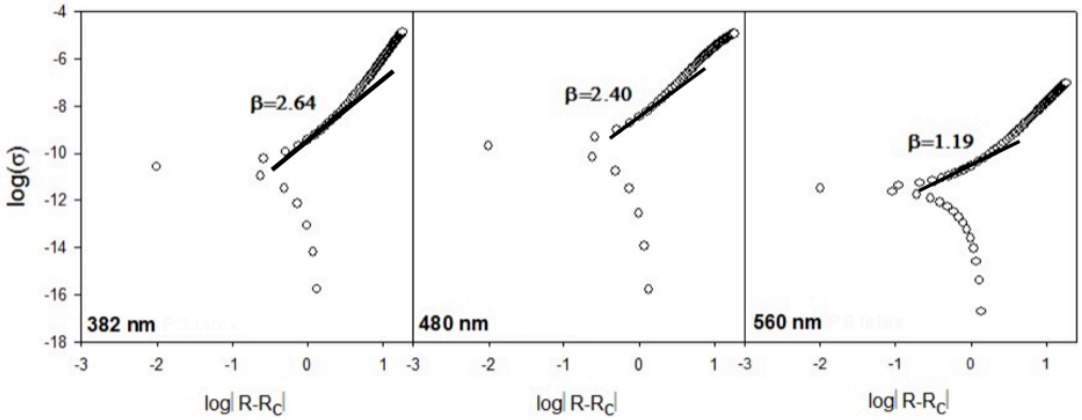

Figure 6.15 : log–log plot of the best fitted curve of σ vs ($|R - R_c|$) for PS/MWCNT nanocomposites.

Lines correspond to the least square fitting of the experimental data with R_c=0.015 (1.5 wt%). The slopes of these lines give β_c=2.64; 2.40 and 1.19 for 382 nm, 480 nm and 560 nm composites, respectively. The percolation thresholds (R_c), critical exponents (β) and quality of fit (R^2) for three composite systems are summarized in Table 6.3. It is clearly observed that all PS/MWCNT systems have the similar percolation threshold, (R_c=1.5 wt%), but different critical exponent (β) values.

Table 6.3 : Percolation thresholds (R_c), critical exponents (β) and quality of fit (R^2) for PS/MWCNT composite systems.

PS size (nm)	R_c (wt%)	β	R^2
382	1.5	2.64	0.99
480	1.5	2.40	0.98
560	1.5	1.19	0.98

Here, it should be noted that β decreases with increasing PS size. The electrical conductivity of the composite systems made from 480 nm and 560 nm particles was higher than that of the composites made of 382 nm particles at all MWCNT contents. In comparison with the 382 nm composite system, it is speculated in the nanocomposite systems of 480 nm and 560 nm that a large network structure connected by nanotube-nanotube links could be formed more densely because the specific surface area of larger PS particles is small (see Figure 6.10). Since the electrical conductivity is affected by the dispersion and distribution state of MWCNTs,

it is speculated that a network structure formed by well dispersed but poorly distributed MWCNTs within an insulating matrix might give higher electrical conductivity. The SEM images indicate the penetration of carbon nanotubes into the PS phase more uniformly through loosely entangled MWCNT bundles (clusters). This results in a decrease in β values and is the order of increase in electrical conductivity of composites with increasing PS particle size. In this work, the value of β obtained for 560 nm composite systems as 1.19 which is close to the theoretically predicted value of $\beta \approx 1.3$, which is evidence of a three-dimensional conductive network of MWCNT into the polymer matrix. However, two critical exponents obtained for 382 nm and 480 nm composite system (β=2.64 and 2.40) exceeds the theoretically predicted value $\beta \approx 2.0$. This effect can be explained by non-statistical ordered distribution of conductive phase in the polymer matrix since the theoretical value of β=2 is provided by the random (statistical) distribution of conductive particles in the non-conductive medium [70].

However, the critical exponents obtained in this study are consistent with the exponents in other studies reported in the literature. It was reported that composites filled with fibers typically have a critical exponent value higher than 2 because of the higher aspect ratio of fibers compared to spheres. For example, in VGCNF/polymer composites, a critical exponent value of 3 was reported for several composites for different types of VGCNFs [71,47]. Similarly, β values in the range of 3 were also reported for SWNT/polymer composites [72,73].

Kim et al. [74] related critical exponent of 2.4 for MWCNT/ PMMA composites. Bauhofer and Kovacs [53] have indicated critical exponent values obtained from experiments for 3-D percolating systems between 1.3 and 4. The range of experimentally determined critical exponent values obtained by different situations indicates that the β is not universal.

6.1.4 Optical percolation behavior of PS/MWCNT nanocomposite films

The transmitted light intensity (I_{tr}) versus MWCNT content is given in Figure 6.16 (I) for three composite film series. Experimental results presented in Figure 6.16 (I) show that I_{tr} decreases with the increase of the MWCNT content. Additionally, as the MWCNT content is increased, I_{tr} decreases continuously to its minimum value (0 %) around 10 wt% of MWCNT for three film series. This indicates that there is almost no

light transmission from the films in all three nanocomposite systems above that of MWCNT content. Here, the addition of MWCNT into PS matrix create a two-phase heterogeneous structure (i. e. the existence of different refractive mediums), which causes light scattering from the composite film surface.

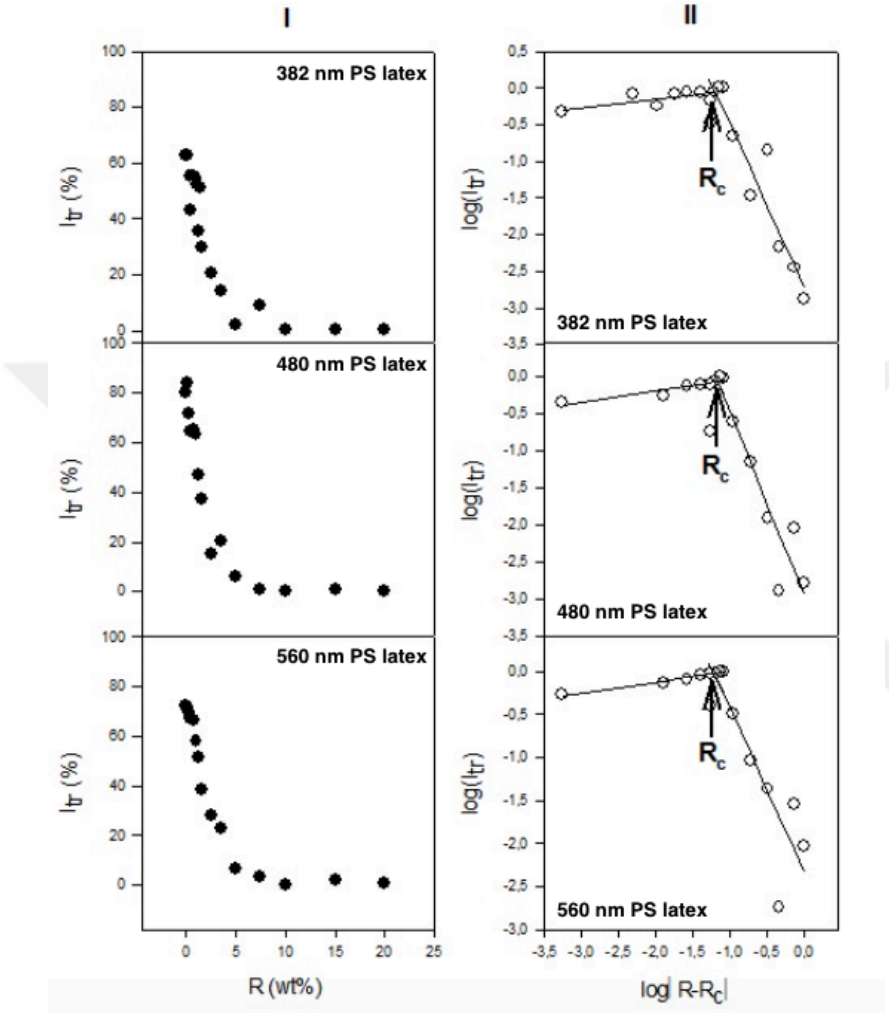

Figure 6.16 : (I) Plot of transmitted photon intensities, I_{tr}, vs. R (wt%) and (II) log-log plot of I_{tr} vs. ($|R - R_c|$) for three film series.

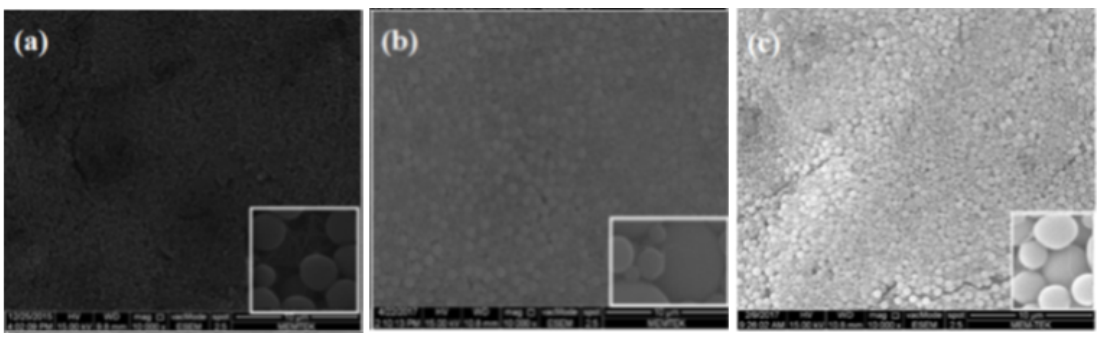

Figure 6.17 : SEM images of nanocomposite films prepared with 10 wt% of MWCNT content before annealing for (a) 382 nm, (b) 480 nm and (c) 560 nm film series. MWCNT bundles are clearly seen in (a).

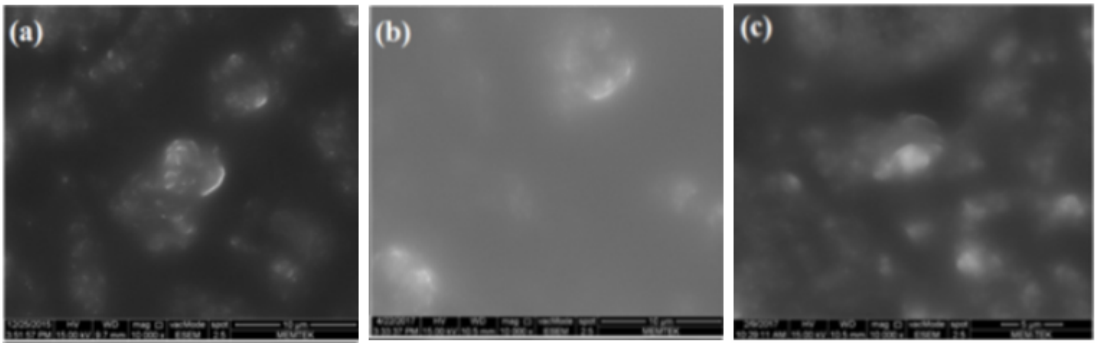

Figure 6.18 : SEM images of nanocomposite films prepared with 10 wt% of MWCNT content annealed at 250 °C for 10 min for (a) 382 nm, (b) 480 nm and (c) 560 nm film series. MWCNT bundles are clearly seen.

This result is also consistent with the microstructural analysis given in Figures 6.17 and 6.18, respectively. The obtained optical transmission data can be treated by the percolation theory assuming that R is identical to lattice occupation probability, P, then percolation threshold value, p_c will be equivalent to R_c. We can assume that the percolation probability, $P_\infty(p)$ is proportional to scattered light intensity $I_{sc} = 1 - I_{tr}$ and then one can arrange the percolation equation (Equation 3.9) for the optical data as follows:

$$I_{sc}(R) \approx (R - R_c)^{\beta_o} \qquad (6.8)$$

Equation 6.8 describes the percolation model for MWCNT distribution in PS lattice where R_c is the critical percolation threshold for MWCNT. Equation 6.8 also describes the percolation model for the distribution of MWNTs in PS lattice where R_c was produced in Figure 6.16 (II) from the intersection of two broken straight lines.

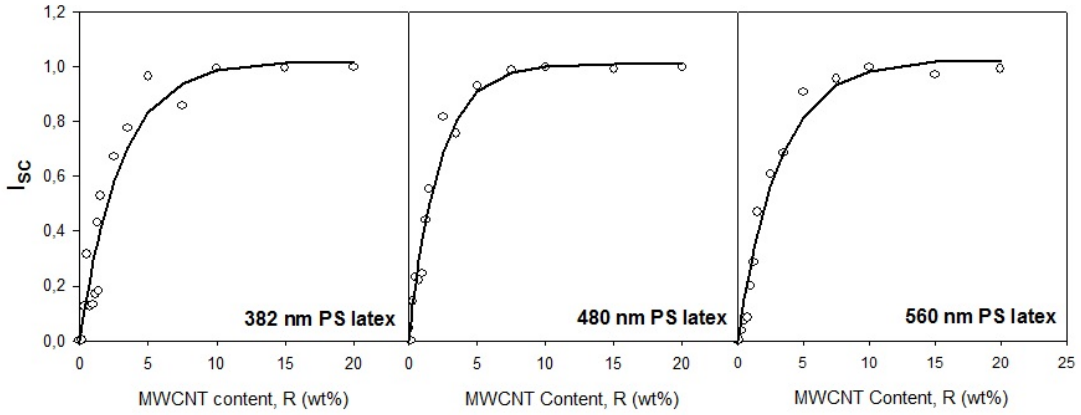

Figure 6.19 : I_{sc} vs. concentration of 382 nm, 480 nm and 560 nm of PS/MWCNT nanocomposite films.

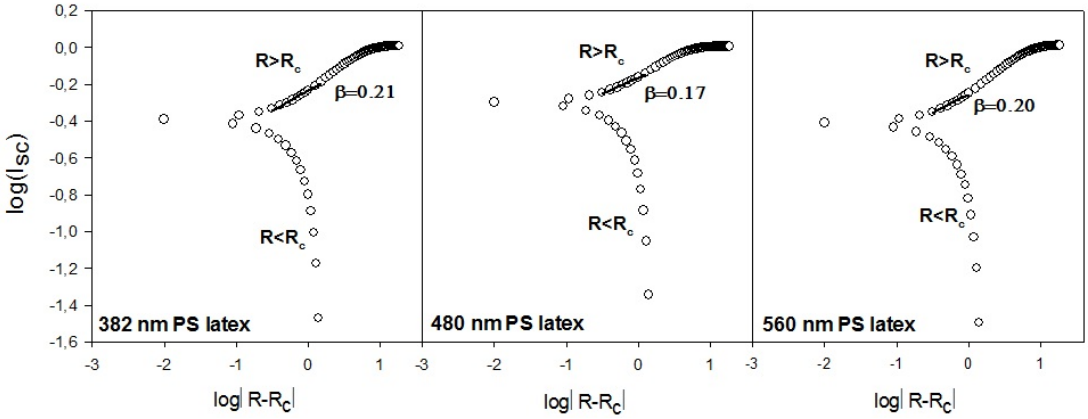

Figure 6.20 : Optical percolations of 382 nm, 480 nm and 560 nm of PS/MWCNT nanocomposite films.

The scattered light intensity, I_{sc} versus MWNTs content and its best fit for all three composite systems, are plotted in Figure 6.19, where it is seen that I_{sc} has increased to larger values for all film samples above 1.5 wt % of MWCNTs content. This behavior of scattering light intensity can be explained by percolating MWCNTs particles in PS lattice. In order to define the R_c value, $\log(I_{sc})$ versus $\log(R)$ was plotted in Figure 6.20. Here, R_c was produced from the intersection of two broken straight lines in these figures and found as R_c=1.5 wt% for all film series.

When R approaches R_c, the largest cluster of MWCNTs appears by connecting the left and right edges to the bottom edge of the MWCNTs. The logarithmic form of Equation 6.8 is fitted to the data in Figure 6.20, where the slopes of the straight lines produced the critical exponents, β_o, above R_c=0.015 which are given in Table 6.4.

Table 6.4 : Percolation thresholds (R_c), critical exponents (β_o) and quality of fit for PS/MWCNT composite systems obtained from optical data.

PS size (nm)	R_c (wt%)	β_o	R^2
382	1.5	0.21 ± 0.096	0.98
480	1.5	0.17 ± 0.056	0.98
560	1.5	0.20 ± 0.097	0.98
Av.	**1.5**	$\mathbf{0.19 \pm 0.083}$	**0.98**

As it is seen from Table 6.4, both R_c and β_o values do not change with PS latex size showing that optical percolation is not affected at all with the increase in PS latex size. However, the produced (average) critical exponent of β_o= 0.19 , above R_c=0.015 for this study is not so far from the bond-percolation theory. In a simple cubic lattice β is found to be 0.25 for the bond percolation model [75].

6.2 PS/GO Nanocomposite Films

6.2.1 Film formation process of PS/GO nanocomposite films

Figure 6.21 shows transmitted light intensities (I_{tr}) versus annealing temperatures for pure PS and PS/GO films for various GO content, respectively. Upon annealing, the transmitted light intensity, I_{tr}, started to increase above a certain onset temperature, called the minimum film-formation temperature T_0, and then reaches a plateau for all film samples. However, for pure PS film (0 wt% of GO), I_{tr} first increases between 100 °C and 130 °C then decreases up to 170 °C. I_{tr} increases again with further annealing above this temperature.

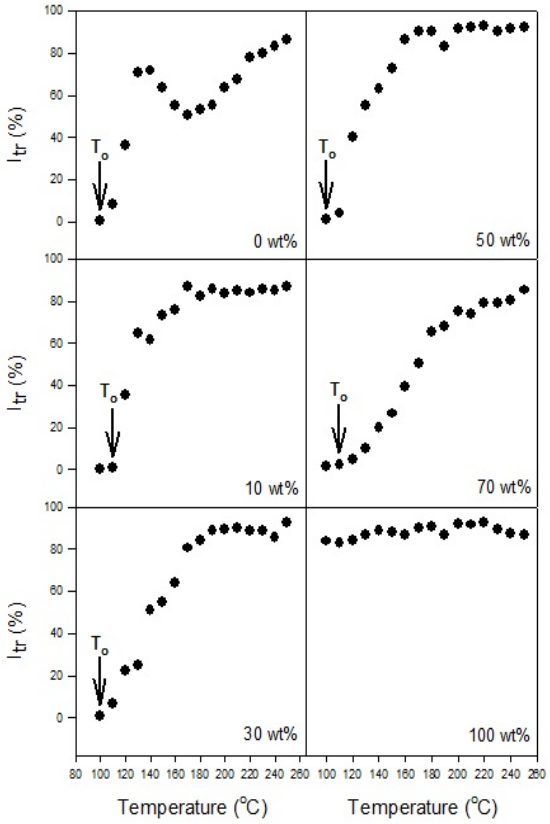

Figure 6.21 : Plots of transmitted photon intensities, I_{tr}, vs. annealing temperatures depending on GO content in PS/GO nanocomposite films.

However, I_{tr} for GO content in films increases consistently with increasing annealing temperature. For all film samples, the increase in I_{tr} above T_0 can be explained by the evaluation of the transparency of the PS films upon annealing. Before annealing, since the film contains many voids (i.e., the high number of polymer–air boundaries) most of the light is scattered at the air–polymer interface yielding low I_{tr} values. Annealing

the films first causes the closure of voids due to the viscous flow of PS polymer and then healing of the particle–particle boundaries [76,77]. Therefore, I_{tr} increases with annealing temperature as shown in Figure 6.21. Furthermore, annealing at higher temperature causes healing and interdiffusion processes, [76,77], respectively, resulting in a more transparent film. On the other hand, the increase in I_{tr} above T_0 presumably corresponds to the void closure process up to the T_h point (see Figure 6.22) where the healing process takes place. The increase in I_{tr} above T_h can be understood by interdiffusion processes between polymer chains [76,77]. Here, the decrease in I_{tr} for pure PS film in Figure 6.21 in the temperature range of 130 °C - 170°C can be explained with the light scattering from the PS aggregations in this film. Due to the negative sulfate groups on the surface of PS latexes, repulsive Coulombic interaction (steric-repulsion) between PS particles occurs during the void closure process at a certain distance.

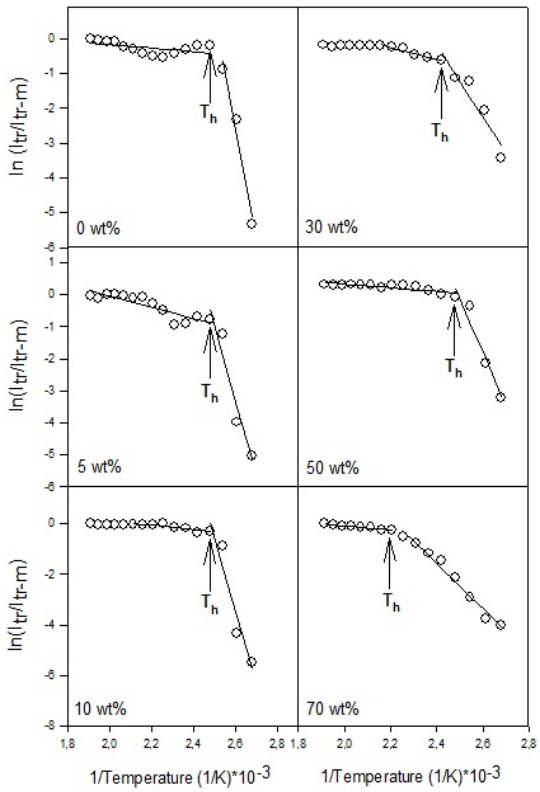

Figure 6.22 : $\ln(I_{tr})$ vs. T^{-1} plots of I_{tr} data in the Figure 6.21. The slope of the straight lines produces ΔH and ΔE activation energies, which are listed in Table 6.5.

This repulsive interaction becomes more pronounced as the particles come closer together during viscous flow which results in PS aggregation. We suggest that the

decrease in I_{tr} above 130 °C for pure PS film is mostly associated with scattering of the light from these aggregations. Then, annealing the films at higher temperatures above 170 °C leads the PS particles to overcome this repulsion and voids are completely closed resulting in increased I_{tr}. At the end of the void-closure process, the particle–particle interfaces are disappeared due to the interdiffusion of polymer chains across the particle-particle interfaces. Then, during interdiffusion, the film becomes more transparent and I_{tr} increases again at annealing temperatures above 170 °C. On the other hand, the steady increase in I_{tr} values of GO content films can be explained by the amphiphilic properties of GO. Since GO involves both hydrophobic (graphenic) areas and numerous hydrophilic (oxygen) functional groups, this makes the GO platelets able to readily absorb surface active molecules on their surface [78]. Most probably, PS particles are attracted by GO platelets due to the Coulombic interaction between the hydrophobic part on the PS particle and the hydrophobic areas in GO, vice versa. Therefore this prevents the repulsion between PS particles. The increase in I_{tr} above T_h originates due to the void closure process, and so Equation 6.3 was applied to I_{tr} for the temperatures between T_h and T_0 for all film samples. Figure 6.22 represents the ln(I_{tr}) versus T^{-1} plots for films from which ΔH activation energies (right hand side) were obtained. The measured ΔH activation energies are listed in Table 6.5. It is seen that ΔH values do not change much by increasing the GO content showing that the amount of heat that was required by one mole of polymeric material to accomplish a jump during viscous flow almost does not change by varying the GO content in the nanocomposite films. The activation energy of backbone motion, ΔE, is produced by least-squares fitting the data in Figure 6.22 (the left hand side) to Equation 6.6, and these are listed in Table 6.5.

Table 6.5 : ΔE, ΔH, T_0 and T_h values of PS/GO nanocomposite films containing different concentrations dried at the room temperature.

GO Content (wt%)	ΔE kJ.mol^{-1}	ΔH kJ.mol^{-1}	T_0 (°C)	T_h (°C)
0.0	1.95	21.80	100	130
3.0	1.08	18.03	110	130
5.0	6.94	15.50	100	130
10.0	2.10	19.01	100	130
20.0	1.08	24.41	110	140
30.0	4.22	9.35	100	140
50.0	2.96	17.69	100	130
70.0	3.27	5.91	110	180

The ΔE values seem almost not to change with increasing GO content, showing that the interdiffusion process is not affected by GO content. In conclusion, the void closure and backbone activation energies for the composite films were found to be similar to the pure latex film. In other words, the presence of GO in the PS latex does not affect the void closure and backbone motion activities.

The behavior of T_0 and T_h also support our findings related to both ΔH and ΔE energies. T_0 is often used to indicate the lowest possible temperature for particle deformation sufficient to decrease interstitial void diameters to sizes well below the wavelength of light [71]. Below this critical temperature, the dry latex is opaque and powdery. However, above this temperature, a latex cast film becomes continuous and clear film [79]. Therefore, T_0 has been considered in this study as the temperature above which the I_{tr} starts to increase. T_h is the healing temperature and indicates the onset of the particle-particle adhesion [79].

Here, T_h is defined as the intersection of two linear regions in Figure 6.22. Both temperatures were determined from the transmittance curves in Figures 6.21 and 6.22 and listed in Table 6.5. As seen from the table, T_0 and T_h temperatures for all film samples does not change as much with increasing the GO content. This result shows that PS latexes in composite films undergo complete film-formation process independent of GO content.

6.2.2 Film morphology of PS/GO nanocomposite films

In order to support the experimental findings, SEM was used to examine the morphologies of PS/GO composite films. Figure 6.23 shows SEM images of the pure PS film annealed at various temperatures. With annealing at 100 °C (Figure 6.23(a)) no deformation in PS particles is observed and a lot of voids are present in the film. After annealing at 130 °C (Figure 6.23(b)), due to the viscous flow voids are disappeared which results increased I_{tr} in Figure 6.21. At 170 °C (the low magnification image in Figure 6.23(c)), where I_{tr} decreased, almost complete void closure is reached but undeformed large spherical PS particles are clearly seen which lead the light scattering. Finally, after annealing the pure PS film at 250 °C, all particles underwent complete film formation and continuous smooth film forms resulting in a transparent film.

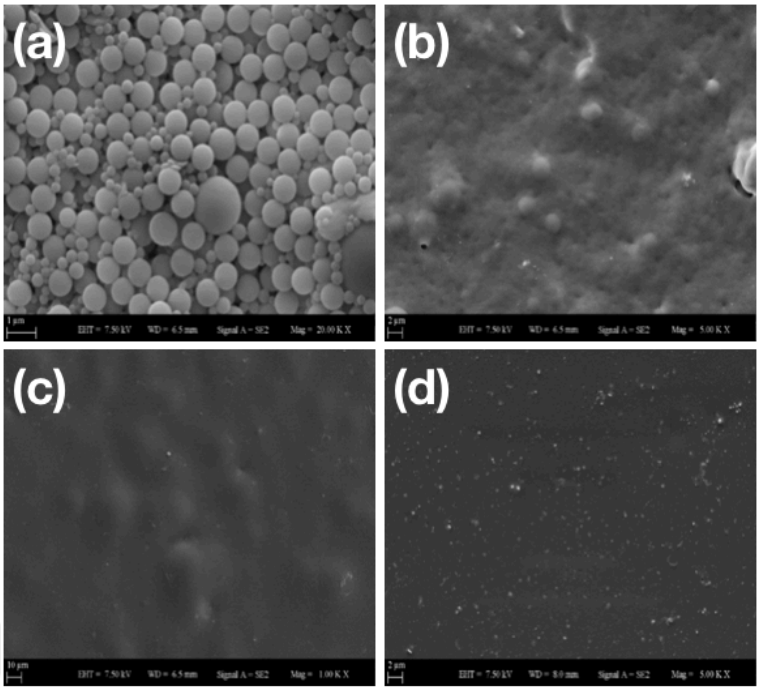

Figure 6.23 : Scanning electron micrographs (SEM) of pure PS latex film annealed at (a) 100, (b) 130, (c) 170, and (d) 250 °C for 10 min.

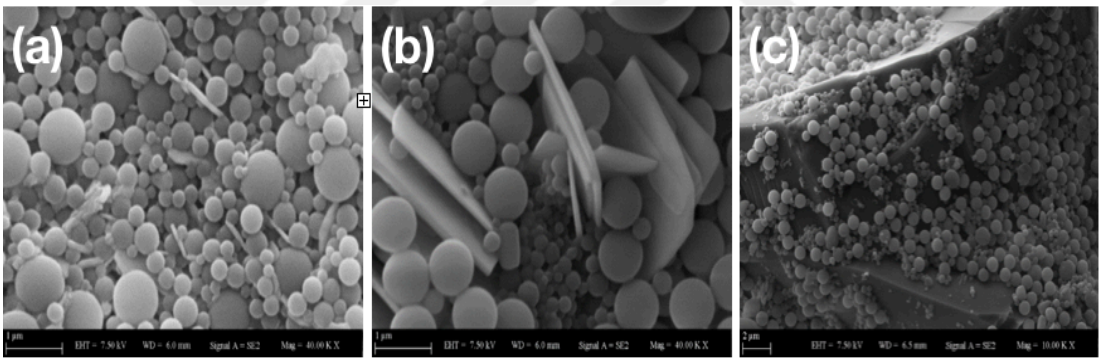

Figure 6.24 : Scanning electron micrographs (SEM) of PS/GO nanocomposite films with (a) 10, (b) 30 and (c) 70 wt% of GO content annealed at 100 °C for 10 min.

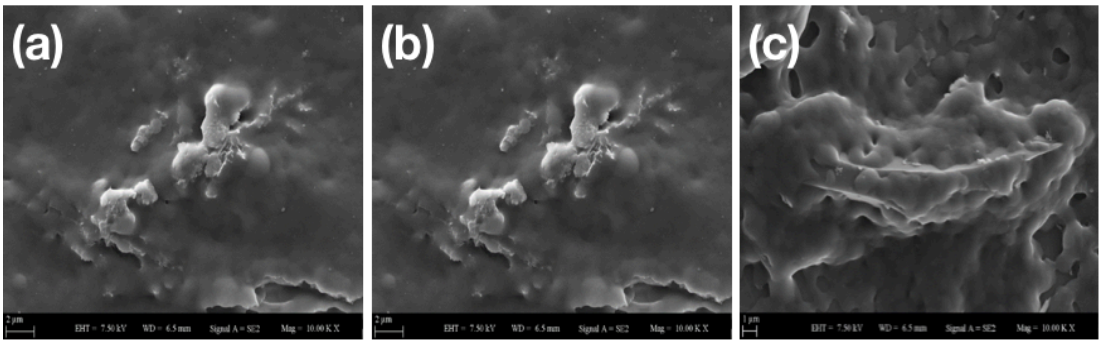

Figure 6.25 : Scanning electron micrographs (SEM) of PS/GO nanocomposite films with (a) 10, (b) 30 and (c) 70 wt% of GO content annealed at 130 °C for 10 min.

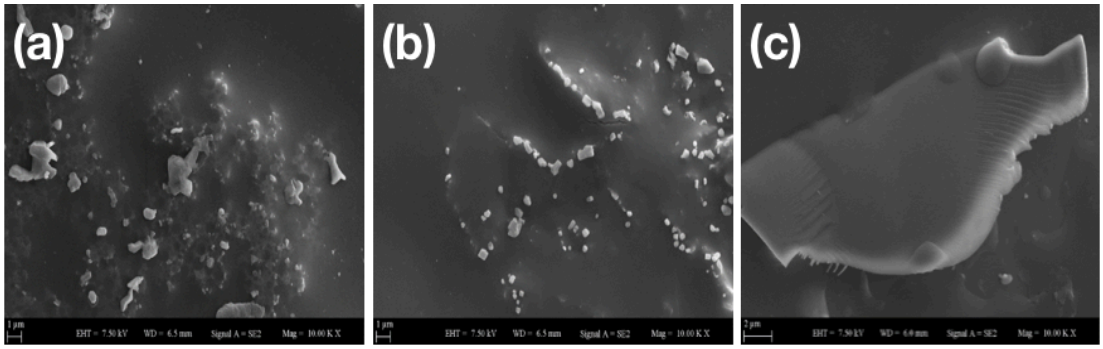

Figure 6.26 : Scanning electron micrographs (SEM) of PS/GO nanocomposite films with (a) 10, (b) 30 and (c) 70 wt% of GO content annealed at 170 °C for 10 min.

Figures 6.24 – 6.27 show SEM images of the PS/GO composite films with 10, 30 and 70 wt% GO content annealed at 100, 130, 170 and 250 °C for 10 min, respectively. At 100°C (see Figure 6.24), composite films show random arrays of PS particles and significant porosity. On the other hand, GO platelets are visible on the surface of the 10 and 30 wt% GO content films. As it is seen in Figures 6.24(a) and 6.24(b), they appear as isolated submicrometer sticks or sheets dispersed within the PS latex matrix.

From these images, it is obvious that the GO sheets are well dispersed all over the film and show no obvious aggregates. However, for 70 wt% of GO content, a large GO block surrounded by PS particles are seen on the surface of the film (see Figure 6.25(c)). This is because during the drying process of the film, the GO tend to aggregate (layer by layer stacking) into rather thick GO flakes. Due to the poor compatibility of the GO and the polymer matrix [80], as the GO content increased to 70 wt% GO, GO sheets are beginning to restack due to the high aspect ratio and strong interparticle interaction [81].

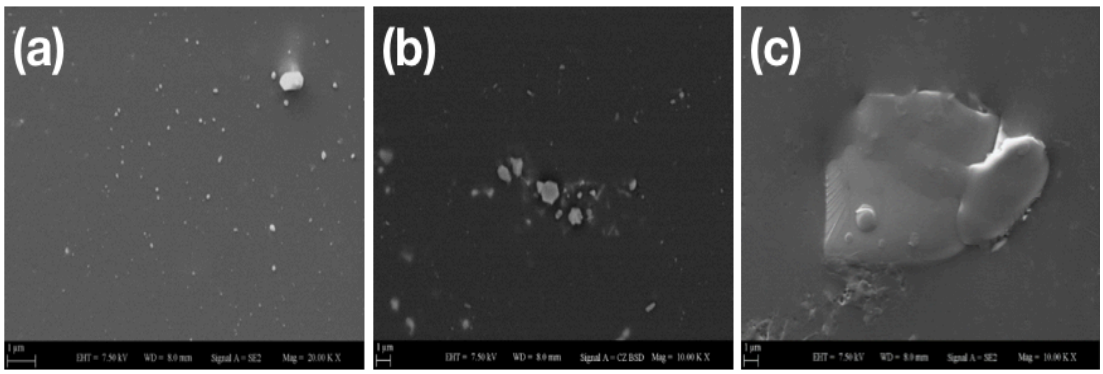

Figure 6.27 : Scanning electron micrographs (SEM) of PS/GO nanocomposite films with (a) 10, (b) 30 and (c) 70 wt% of GO content annealed at 250 °C for 10 min.

In addition, PS particles are seen attached to the surface of GO block due to the Coulombic attraction between GO and PS particles. Here, at this stage of film formation, the morphology of composites are seen strongly influenced by increasing the GO content in the film.

Upon annealing the films at 130 °C (see Figure 6.25), the polymeric particles packed closely on the GO sheets forming a compact structure. This could be responsible for the increased I_{tr} in Figure 6.21 for GO content films. As seen in Figure 6.26, after annealing at 170 °C, all the nanocomposite films exhibit relatively homogeneous and smooth surfaces. It is possible to distinguish that the GO sheets in 10 and 30 wt% GO content films are completely covered with PS polymer.

On the other hand, despite the smooth surfaces of the films, GO particles and/or large GO sheets are still visible on the surface of the films. At 250 °C (see Figure 6.27), film surfaces become flatter and more continuous, which is similar to that observed for neat PS latex. This indicates that the complete film formation of PS particles took place and GO sheets are completely embedded into PS polymer phase. However, a large GO sheet partially embedded in PS phase still appears on the surface of 70 wt% GO content film.

6.2.3 Electrical conductivity of PS/GO nanocomposite films

Figure 6.28(a) shows electrical conductivity (σ) of PS/GO composite films as a function of GO content annealed at 250 °C. Interestingly, the conductivity decreases slightly with increasing GO content. It is seen that the addition of the GO nanofiller in the polymer film decreases the conductivity about one order of magnitude from 10^{-13} S to 10^{-14} S in comparison with the pure polymer. This decrease may be due to the surface morphology of PS/GO and the incorporation of rather large electrically non-conducting GO flakes into the film with increasing GO content.

It is well known that GO is the oxidation product of graphene and has many oxygen-containing functional groups which could introduce defects to graphene [82]. However, it has been demonstrated that the electrical conductivity of GO could be significantly recovered by chemical reduction [82,88], restoring a graphitic network of sp^2 bonds.

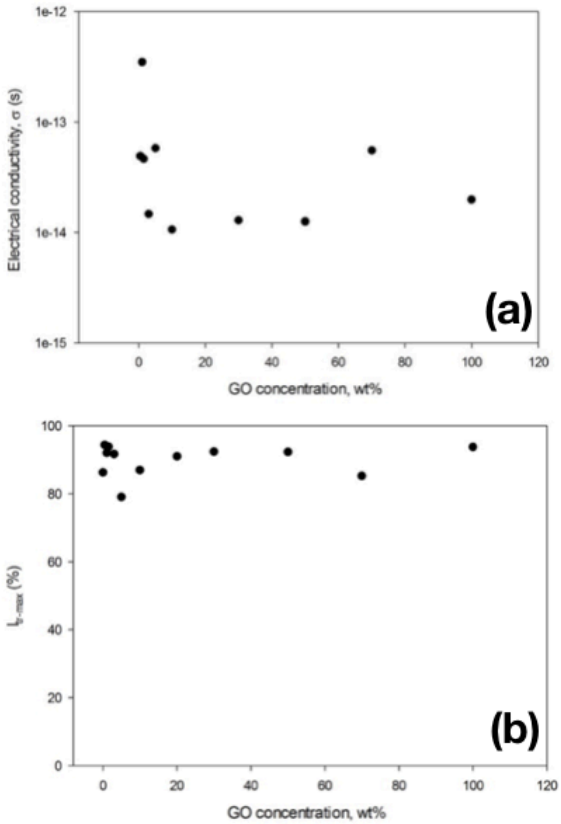

Figure 6.28 : (a) Electrical properties and (b) optical transmission, $(I_{tr})_m$ of PS/GO composite films annealed at 250 °C as a function of GO content.

It has been shown that when GO is heated above 200 °C, deoxygenation occurs in GO as result of the thermal reduction. But in our case annealing the films at 250 °C seems not to produce any significant change in the electrical conductivity of PS/GO composite films. The nanocomposite films exhibit dielectric behavior with quite low conductivity values, in the order of 10^{-13} -10^{-14} S. Finally, in order to see the change in the optical transparency of the films with GO content, the transmitted light intensity of the composite films annealed at 250 °C was plotted in Figure 6.28(b). Film transparency is almost not affected by increasing GO content from 0 to 100 wt%. The transparency of the films is quite high and almost about 90%. This shows that it is possible to prepare highly transparent dielectric materials with a simple and cheap method used in this study.

7. CONCLUSION

The PS/MWCNT nanocomposites were prepared via latex technology and the effects PS particle size and MWCNT content on film formation and electrical properties of these composites were investigated. Three different PS particles with different diameters (382 nm, 480 nm and 560 nm) were synthesized by emulsion polymerization. Films were prepared by the drop-casting method at room temperature and annealing them at temperatures above glass transition temperature, T_g of PS between 100 °C and 250 °C for 10 min. The nanocomposites made with 382 nm particle underwent complete film formation in the (0-7.5) wt% of MWCNT range whereas nanocomposites made with 480 nm and 560 nm particle sizes accomplished the film formation process in the presence of (0-5) wt% of MWCNT. For MWCNT concentration above these ranges film formation of PS latexes was not monitored due to the light scattering from MWCNT bundles in the films. A similar percolation threshold, R_c (which is 1.5 wt% of MWCNT) was found for all nanocomposite film systems, whereas critical exponent decreased as the particle size of PS increased. However, the electrical conductivity increased one order of magnitude as the latex particle size was increased from 382 nm to 560 nm. The nanocomposite prepared by large particles showed higher electrical conductivity as the MWCNT content increased. It is speculated that large PS particles are more effective at all MWCNT content because sparsely linked but densely connected electrical pathway could be built. SEM images showed characteristic differences between the microstructure of the three composite systems as the MWCNT concentration is increased. From these images it was seen that 382 nm latex system coaleses and envelops the MWCNT bundles very well at higher MWCNT concentrations reducing the porosity that accompanies complete coalescence. However, nanocomposites made with 480 nm and 560 nm latexes fail to completely coalesces at higher MWCNT concentrations which create microvoids. MWCNTs do not appear to significantly interact with the latex-based matrix, which contributes to stronger networks and higher electrical conductivity. The latex mixing was also method was used to prepare PS/GO

nanocomposites, and the effect of the GO content on the the film formation process was studied by using photon transmission technique. The morphology of nanocomposites was also studied by considering SEM, and the electrical properties of the films were measured by two probe technique. Nanocomposite films were prepared by mixing of PS latex particles and GO solution with various weight ratio. These films were then annealed at elevated temperatures in the range of 100 °C - 250 °C to study film the formation process. From the optical transmission and SEM results, it was observed that classical latex film formation occurred for all GO content films. Both ΔH and ΔE activation energy values obtained from optical data were found not to change with increasing GO content in the films indicating that GO has no influence on the film formation process of PS/GO composites which is also confirmed by the SEM images. Although its high transparency (90%), no change in the electrical conductivity of PS/GO composite films was observed and they exhibited dielectric behavior. In conclusion, our approach which was aimed in this study is to develop a cheap, simple and an effective method for the preparation of high performance dielectric nanocomposites which can be used in diverse application fields of dielectric materials. Based on the results of this study, as a future work, we shall study the effect the oxidation degree of GO sheets on both film formation and electrical properties (for the conductivity enhancement) and on thermal stability of polymer/GO nanocomposite films. For this purpose, the chemically reduced GO will be prepared from commercial GO aqueous dispersions at different C:O ratios of GO. In order to prevent the drop in solubility of reduced GO in water, surfactants or water-soluble polymers will also be used for the stabilization of GO. Much more experiments will be conducted to optimize the experimental parameters such as oxidation degree, the ratio of GO to the stabilizer and/or polymer latex, annealing temperature and so forth.

8. REFERENCES

[1] **Paul, D. R., Robeson, L. M.** (2008). Polymer technology: Nanocomposites, *Polymer*, *49*, 3187-3204.

[2] **Saini, R., Saini, S., Sharma, S.** (2010). Nanotechnology: The future medicine, *Journal of Cutaneous and Aesthetic Surgery, 3*, 32-33.

[3] **Das, I., Ansari, S. A.** (2009). Nanomaterials in science and technology, *Journal of Scientific & Industrial Research*, *68*, 657-667.

[4] **Hübler, A. W., Osuagwu, O.** (2010). Digital quantum batteries: Energy and information storage in nanovacuum tube arrays, *Complexity*, *15*, 48-55.

[5] **Mathew, D. S., Juang, R. S.** (2007). An overview of the structure and magnetism of spinel ferrite nanoparticles and their synthesis in microemulsions, *Chemical Engineering Journal*, *129*, 51-65.

[6] **Gleiter, H.** (2000). Nanostructured materials: basic concepts and microstructure, *Acta Materiala*, *48,* 1-29.

[7] **Skorokhod, V., Ragulya, A., Uvarova, I.** (2001). Physico-chemical kinetics in nanostructured systems, *Kyiv: Academperiodica*, *1*, 180.

[8] **Pokropivny, V. V., Skorokhod, V. V.** (2007). Classification of nanostructures by dimensionality and concept of surface forms engineering in nanomaterial science, *Materials Science and Engineering: C*, *27*, 990-993.

[9] **Kim, Y. T., Han, J. H., Hong, B. H., Kwon, Y. U.** (2010). Electrochemical synthesis of CdSe quantum-dot arrays on a graphene basal plane using mesoporous silica thin-film templated, *Advanced Materials*, *22*, 515-518.

[10] **Tiwari, J. N., Tiwari, R. N., Kim, K. S.** (2012). Zero-dimensional, one-dimensional, two-dimensional and three-dimensional nanostructured materials for advanced electrochemical energy devices, *Progress in Materials Science*, *57*, 724-803.

[11] **Nayak, B. B., Behera, D., Mishra, B. K.** (2010). Synthesis of silicon carbide dendrite by the arc plasma process and observation of nanorod bundles in the dendrite arm, *Journal of the American Ceramic Society*, *93*, 3080-3083.

[12] **Wang, L., Yamauchi, Y.** (2009). Facile synthesis of three-dimensional dendritic platinum nanoelectrocatalyst, *Chemistry of Materials*, *21*, 3562-3569.

[13] **Camargo, P. H. C., Satyanarayana, K. G., Wypych, F.** (2009). Nanocomposites: synthesis, structure, properties and new application opportunities, *Materials Research, 12*, 1-39.

[14] **Saritha, A., Joseph, K., Boudenne, A., Thomas, S.** (2011). Mechanical, thermophysical, and diffusion properties of TiO2-filled chlorobutyl rubber composites, *Polymer Composites*, *32*, 1681–1687.

[15] **Xue, Q., Sun, J.** (2016). Electrical conductivity and percolation behavior of polymer nanocomposites. In X. Huang, C. Zhi (Eds.), *Polymer Composites* (Vol. 1, pp.51-82). New York: Springer.

[16] **Hussain, F., Hojjati, M., Okamoto, M., Gorga, R. E.** (2006). Polymer-matrix nanocomposites, processing, manufacturing, and application: an overview, *Journal of Composite Materials*, *40,* 1512-1575.

[17] **Anandhan, S., Bandyopadhyay, S**. (2011). Polymer Nanocomposites: From synthesis to applications, In J. Cuppoletti (Eds.), *Nanocomposites and Polymers with Analytical Methods* (Vol. 1, pp.1-28). Retrieved from: https://www.intechopen.com/books/nanocomposites-and-polymers-with-analytical-methods/polymer-nanocomposites-from-synthesis-to-applications

[18] **McCrum, N. G., Buckley, C. P., Bucknall, C. B.** (1996). Principles of Polymer Engineering, New York: Oxford Science.

[19] **Yuan, Q., Misra, R. D. K**. (2006). Polymer nanocomposites: current understanding and issues, *Materials Science and Technology*, *22*, 742-755.

[20] **Pekcan, Ö., Adıyaman, N., Uğur, Ş.** (2002). Energy-Transfer Method to study vapor-induced latex film formation, *Journal of Applied Polymer Science*, *84*, 632-645.

[21] **Kedide, J. K.** (1997). Film Formation of Latex, *Materials Science and Engineering*, *21*, 101-170.

[22] **Yargı, Ö.** (2010). *Polimer kompozitlerden film oluşumu ve oksijen geçirgenliği* (Ph.D. Thesis). Istanbul Technical University, Institute of Science and Technology, İstanbul.

[23] **Uğur, Ş., Elissari, A., Pekcan, Ö.** (2003). Void closure and interdiffusion processes during latex film formation from surfactant-free polystyrene particles: a fluorescence study, *Journal of Colloid and Interface Science*, *263*, 674-683.

[24] **Uğur, Ş., Pekcan, Ö.** (2005). Percolation approach to film formation from surfactant-free polystyrene particles, *Phase Transitions*, *78*, 593-606.

[25] **Ramoa, S. D., Barra, G. M., Oliveira, R. V., De Oliveira, M. G., Cossa, M., Soares, B. G.** (2013). Electrical, rheological and electromagnetic interference shielding properties of thermoplastic polyurethane/carbon nanotube composites, *Polymer International*, *62*, 1477–1484

[26] **Kattimuttathu, S. I., Krishnappan, C., Vellorathekkaepadil, V., Nutenki, R., Mandapati, V. R., Cernik, M.** (2015). Synthesis, characterization and optical properties of graphene oxide-polystyrene nanocomposites, *Polymers for Advanced Technology*, *26*, 214-222.

[27] **Kim, H., Macosko, C. W.** (2009). Processing-property relationships of polycarbonate/graphene composites, *Polymer*, *50*, 3797–3809.

[28] **Kuilla, T., Bhadra, S., Yao, D., Kim, N. H., Bose, S., Lee, J. H.** (2010). Recent advances in graphene based polymer composites, *Progress in Polymer Science*, *35,* 1350–1375.

[29] **Uğur, Ş., Yildiz, O., Kara, S.** (2017). Investigation of film formation and electrical properties of PS Latex/MWCNT Nanocomposites, In F.M. Lucas (Eds.)*, Materials Design and Applications* (Vol. 65, pp.79-100). Switzerland: Springer.

[30] **Chaineg, M., Wilkinson, M. C., Hearn, J**. (1985). Film formation of waterborne PUs, *Journal of Polymer Science*, *23*, 2947.

[31] **Dobler, F., Pith, T., Lambla, M., Holl, Y.** (1992). Coalescence mechanisms of polymer colloids: II. Coalescence with evaporation of water, *Journal of Colloid and Interface Science, 152*, 12-21.

[32] **Keddie, J. L., Meredith, P., Jones, R. A. L., Donald, A. M.** (1996). Film formation in waterborne coatings, *Journal of American Chemical Society*, *648*, 332-348.

[33] **Mc Kenna, G. B.** (1989). In Comprehensive Polymer Science, Oxford, UK: Pergamon Pres.

[34] **Vogel, D. H.** (1925). Das temperaturabhaengigkeitsgesetz der viskositaet von fluessigkeiten, *Physikalische Zeitschrift*, *22*, 645-646.

[35] **Fulcher, G. S.** (1925). Analysis of recent measurements of the viscosity of glasses, *Journal of American Ceramic Society*, *8,* 339-355.

[36] **Frenkel, J.** (1945). Viscous flow of crystalline bodies under the action of surface tension*, Journal of Physics*, *9*, 385-391.

[37] **Pekcan, O., Arda, E.** (1998). Effect of molecular weight on latex film formation: photon transmission study, *Journal of Applied Polymer Science, 70,* 339-351.

[38] **Pekcan, O., Arda, E., Bulmus, V., Piskin, E.** (2000). Photon transmission method for studying film formation from polstyrene latexes with different molecular weights, *Journal of Applied Polymer Science*, *77*, 866-874.

[39] **Arda, E., Ozer, F., Piskin, E., Pekcan, O.** (2001). Film formation from nanosized copolymeric latex particles, *Journal of Colloid and Interface Science, 233*, 271-279.

[40] **Arda, E., Pekcan, O.** (2001). Time and temperature dependence of void closure, healing and interdiffusion during latex film formation, *Polymer*, *42*, 7419-7428.

[41] **Ugur, S., Yargi, O., Pekcan, O.** (2008). Film formation from PS latex doped PNIPAM hydrogels at various heating and cooling rates, *Composite Interface*, *15*, 411–424.

[42] **Prager, S., Tirrell, M.** (1981). The healing process at polymer-polymer interfaces, *The Journal of Chemical Physics*, *75*, 5194–5198.

[43] **de Gennes, P. G.** (1982). Kinetics of diffusion-controlled processes in dense polymer systems. II. Effects of entanglements, *The Journal of Chemical Physics, 76*, 3322–3326.

[44] **Li, C., Thostenson, E. T., Chou, T. W.** (2008). Sensors and actuators based on carbon nanotubes and their composites: a review, *Composites Science and Technology*, *68*, 1227–1249.

[45] **Stauffer, D., Aharony, A.** (1994). Introduction to Percolation Theory, London: Taylor&Francis.

[46] **Broadbent, S. R., Hammersley, J. M.** (1957). Percolation processes. I. Crystal and mazes, *Proceedings of the Cambridge Philosophical Society, 53*, 629-641.

[47] **Sahimi, M.** (1994). Applications of Percolation Theory, London: Taylor and Francis,

[48] **Weber M, Kamal M. R.** (1997). Estimation of the volume resistivity of electrically conductive composites, *Polymer Composites*, 1997, *18,* 711–725.

[49] **Sandler, J. K., Kirk, W., Kinloch, J. E., Shaffer, M. S. P., Windle, A. H.** (2003). Ultra-low electrical percolation threshold in carbon-nanotube-epoxy composites, *Polymer*, *44* , 5893-5899.

[50] **IIjima, S.** (1991). Helical microtubules of graphitic carbon, *Nature, 354,* 56-58.

[51] **Bauhofer, W., Kovacs, J. Z.** (2009). A review and analysis of electrical percolation in carbon nanotube polymer composites, *Composites Science and Technology, 69*, 1486-1498.

[52] **Schadler, L. S., Giannaris, S. C., Ajayan, P. M.** (1998). Load transfer in carbon nanotube epoxy composites, *Applied Physics Letters, 73,* 3842-3844.

[53] **Gojny, F. H., Wichmann, M. H. G., Fiedler, B. Kinloch, I. A., Bauhofer, W., Windle, A. H., Schulte, K.** (2006). Evaluation and identification of electrical and thermal conduction mechanisms in carbon nanotube/epoxy composites, *Polymer, 47,* 2036-3045.

[54] **McNally, T., Pötschke, P., Halley, P., Murphy, M., Martin, D., Bell, S. E. J., Brennan, G. P., Bein, D., Lemoine, P., Quinn, J. P.** (2005). Polyethylene multiwalled carbon nanotube composites, *Polymer, 46,* 8222-8232.

[55] **Stadermann, M., Papadakis, S. J., Falvo, M. R., Novak, J., Snow, E., Fu, Q., Liu, J., Fridman, Y., Boland, J. J., Superfine, R., Washburn S.** (2004). Nanoscale study of conduction through carbon nanotube networks, *Physical Review B, 69,* 1-3.

[56] **Grossiord, N., Wouters, M. E. L., Miltner, H. E., Lu, K., Loos, J., Mele, B. V., Koning, C. E.** (2010). Isotactic polypropylene/ carbon nanotube composites prepared by latex technology: electrical conductivity study, *European Polymer Journal, 46,* 1833-1843.

[57] **Kim, S. T., Choi, H. J., Hong, S. M.** (2007). Bulk polymerized polystyrene in the presence of multi-walled carbon nanotubes, *Colloid and Polymer Science, 285,* 593-598.

[58] **Zannotti, M., Giovannetti, R., D'Amato, C. A., Rommozzi, E.** (2015). Spectroscopic studies of porphyrin functionalized multiwalled carbon nanotubes and their interaction with TiO2 nanoparticles surface,

Spectrochimica Acta Part A: Molecular and Biomolecular Spectroscopy, *153*, 22-29.

[59] **Url-1** <www.cheaptubes.com> , date retrieved 20.05.2017.

[60] **Zhao, H. J., Yao, M., Chen, Q., Wang, D., Wan, L. J.** (2010). Theoretical understanding of adlayer structure, thermal stability and electronic property of graphene molecules, *Surface Science, 604*, 2091−2097.

[61] **Voloshina, E. N., Mollenhauer, D., Chiapposi, L., Paulus, B.** (2011). Theoretical study on the absorption of pyridine derivatives on graphene, *Chemical Physics Letters, 510*, 220−223.

[62] **Song, B., Li, D., Qi, W. P., Elstner, M., Fan, C., Fang, H. P.** (2010). Graphene on Au(111): A highly conductive material with excellent adsorption properties for high-resolution bio/nanodetection and identification, *ChemPhysChem*, *11*, 585−589.

[63] **Ito, A., Wang, Y., Irle, S., Morokuma, K., Nakamura, H. J.** (2009). Molecular dynamics simulation of hydrogen atom sputtering on the surface of graphite with defect and edge, *Journal of Nuclear Materials*, *390*, 183-187.

[64] **Malhotra, B., Srivastava, S., Augustine, S.** (2015). Biosensors for food toxin detection: carbon nanotubes and graphene, *Materials Research Society Symposium Proceedings*, *1725*, 165-175.

[65] **Arda, E., Kara, S., Pekcan, Ö**. (2012). Electrical, optical and fluorescence percolations in P(VAc-co-BuA)/MWCNT composite films, *Phase Transitions*, *86*, 1017-1032.

[66] **Sandler, J., Shaffer, M. S. P., Prasse, T., Bauhofer, W., Schulte, K., Windle, A. H.** (1999). Development of a dispersion process for carbon nanotubes in an epoxy matrix and the resulting electrical properties, *Polymer*, *40*, 5967.

[67] **Liu, J. S., Feng, J., Winnik, M. A.** (1994). Study of polymer diffusion across the interface in latex films through direct energy transfer experiments, *The Journal of Chemical Physics, 101*, 9096-9103.

[68] **Pekcan, O., Arda, E.** (2002). Interfacial behavior of latex films, In P. Somasundaran (Eds.), *Encyclopedia of Surface and Colloid Science* (Vol. 5, p.2691), New York: Marcel and Dekker.

[69] **Keddie, J. L., Meredith, P., Jones, R. A. L., Donald, A. M. (**1995). Kinetics of Film Formation in Acrylic Latices Studied with Multiple-Angle-of-Incidence Ellipsometry and Environmental SEM, *Macromolecules*, *28*, 2673-2682.

[70] **Lux, F.** (1993). Models proposed to explain the electrical conductivity of mixtures made of conductive and insulating materials, *Journal of Material Science, 28*, 285–301.

[71] **Finegan, I. C., Tibbetts, G. G.** (2001). Electrical conductivity of vapor grown carbon fiber/thermoplastic composites, *Journal of Materials Research, 16*, 1668–1674.

[72] **Li, N., Huang, Y., Du, F., He, X. B., Lin, X., Gao, H. J.** (2006). Electromagnetic interference (EMI) shielding of singlewalled carbon nanotube epoxy composites, *Nano Letters*, *6*,1141–1150.

[73] **Bryning, M. B., Islam, M. F., Kikkawa, J. M., Yodh, A. G.** (2005). Very low conductivity threshold in bulk isotropic single-walled carbon nanotube–epoxy composites, *Advanced Materials*, *17*, 1186–1191.

[74] **Kim, H. M., Kim, K., Lee, S. J., Joo, J., Yoon, H. S., Cho, S. J.** (2004). Charge transport properties of composites of multiwalled carbon nanotube with metal catalyst and polymer: application to electromagnetic interference shielding, *Current Applied Physics*, *4*, 577-580.

[75] **Overbeek, A.** (2011). Polymer heterogeneity in waterborne coatings, *Journal Coatings Technology and Research*, 7, 1-21.

[76] **Ugur, S., Elaissari, A., Pekcan, O.** (2003). Void closure and inter-diffusion processes during latex film formation from surfactant-free polystyrene particles: a fluorescence study, *Journal of Colloid and Interface Science*, *263*, 674-683.

[77] **Ugur, S., Elaissari, A., Pekcan, O.** (2004). Film formation from surfactant-free, slightly crosslinked, fluorescein-labeled polystyrene particles, *Journal of Coatings Technology and Res*earch, *1*, 305-313.

[78] **Stankovich, S.** (2006). Stable aqueous dispersions of graphitic nanoplatelets via the reduction of exfoliated graphite oxide in the presence of poly(sodium 4-styrenesulfonate), *Journal of Materials Chemistry, 16*, 155-158

[79] **Eckersley, S. T., Rudin, A.** (1990). Mechanism of film formation from polymer latexes, *Journal of Coatings Technology and Research*, *62*, 89-100.

[80] **Pan, S., Aksay, I. A.** (2011). Factors controlling the size of graphene oxide sheets produced via the graphite oxide route, *ACS Nano*, *5*, 4073–4083.

[81] **Stankovich, S., Dikin, D. A., Dommett, G. H. B., Kohlhaas, K. M., Zimney, E. J., Stach, E. A., Piner, R. D., Nguyen, S. T., Ruoff, R. S.** (2006). Graphene-based composite materials, *Nature*, *442*, 282–286.

[82] **Eda, G., Chhowalla, M.** (2010). Chemically derived graphene oxide: Towards large-area thin-film electronics and optoelectronics, *Advanced Materials*, *22*, 2392–2341.

CURRICULUM VITAE

Name Surname	**: Barış Demirbay**
Place and Date of Birth	**: İstanbul / 29.04.1991**
E-Mail	**: demirbay@itu.edu.tr**

EDUCATION :

- **B.Sc.** : 2015, İstanbul Technical University, Faculty of Science and Letters, Department of Physics Engineering

PROFESSIONAL EXPERIENCE AND REWARDS:

- Graduation Award (Graduated as 3rd best student of class '15)
- The 3rd Best Poster Award – Poster Title: The Effect of Dextran and Dextrin to Viscosity for Biomedical Applications, Balaton Summer School in Physics, 2017

PUBLICATIONS, PRESENTATIONS AND PATENTS ON THE THESIS:

- **Demirbay, B., Uğur Ş.** 2017. Experimental Investigation of Morphological and Electrical Characteristics of PS/MWCNT Nanocomposite Films, *Materials Science Forum.* (Accepted Article)
- **Demirbay, B., Uğur Ş.** 2017. Investigation of the Effect of Graphene Oxide (GO) Nanofillers on Film Formation of Polystyrene (PS) Latex/GO composites, *Polymer Composites*. (Submitted Article)
- **Demirbay, B., Kara S., Uğur Ş.** 2017. Film Formation, Morphological and Electrical Percolation Behavior of PS/MWCNT Nanocomposite Films Containing Different PS Particle Sizes, *Polymer Composites*. (Article-will be submitted)
- **Demirbay B., Uğur Ş.** 2017. The Size Effect of Polystyrene (PS) latexes on Film Formation Process and Electrical Properties of Multi-Walled Carbon Nanotube Doped (MWCNT) PS/MWCNT Nanocomposite Films. Tenth Japanese-Mediterranean Workshop on Applied Electromagnetic Engineering for Magnetic, Superconducting, Multifunctional and Nanomaterials, July 4-8, 2017 İzmir, Turkey. (Oral Presentation)
- **Demirbay, B., Uğur Ş.** 2017. The Effect of PS Particle Size on Morphological, Electrical and Optical Percolation Properties of PS/MWCNT nanocomposite films, *Colloid and Polymer Science*. (Submitted Article)

OTHER PUBLICATIONS, PRESENTATIONS AND PATENTS:

- **Demirbay, B., Akaoğlu C., Ayhan A.A., Acar F.G.** 2017. The Role of Hydrophilic Glucose and Sodium Chloride Molecules on Mechanical

Characteristics of Gelatin Based Films at Various Concentrations: A Study of Tensile Testing, *Canadian Journal of Physics*. (Submitted Article)

- **Demirbay B., Ayhan A.A., Cereyan N., Akaoğlu C., Ulusaraç I., Koyuncu N., Acar F.G.** 2017. Rheological Properties of Dextrin Based Riboflavin Solutions Under Thermal and UV Radiation Effects, *Journal of Molecular Liquids*, *240*, 567-603. (Article)
- **Demirbay B., Akaoğlu C., Ulusaraç I., Acar F.G.** 2017. Thermal and UV Radiation Effects on Dynamic Viscosity of Gelatin-Based Riboflavin Solutions, *Journal of Molecular Liquids*, *225*, 147-150. (Article)
- **Cereyan N., Demirbay B., Akaoğlu C., Acar F.G.** 2016. The Effect of Dextran and Dextrin to Viscosity for Biomedical Applications, 12th Nanoscience and Nanotechnology Conference. (Poster Presentation)
- **Koyuncu N., Ulusaraç İ., Demirbay B., Acar F.G.** 2016. Viscosity Properties of Biocompatible Gelatinous Solutions with Glucose and Sodium Chloride, 2th International Organic Electronic Material Conference. (Poster Presentation)
- **Demirbay B., Çetin T., Fırat E.D., Acar F.G.** 2016. From Effluvium Olive Mill Wastewater (OMW) to Salubrious Gelatin Based OMW Films, Recent Advances in Energy, Environment and Financial Science, 202-204. (Conference Paper)
- **Demirbay B., Akın Evingür G., Acar F.G.** 2015. Investigation of Mechanical Properties of a Biocompatible Film from Riboflavin and Gelatin, Recent Advances on Biomedical Sciences, 88-90. (Conference Paper)
- **Demirbay B., Acar F.G.** 2015. The Viscosity Behavior of Biocompatible Solutions Including Riboflavin and Gelatin, Recent Advances on Biomedical Sciences, 91-94. (Conference Paper)